

Oil & Natural Gas Technology

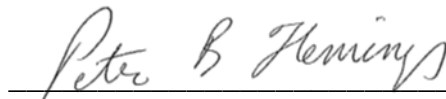
DOE Award No.: DE-FE0010406
DUNS No.: 170230239

Quarterly Research Performance Progress Report (Period ending 12/31/2013)

CONTROLS ON METHANE EXPULSION DURING MELTING OF NATURAL GAS HYDRATE SYSTEMS: TOPIC AREA 2

Project Period (9/30/2013 to 12/31/2013)

Submitted by:
Peter B. Flemings



Signature

The University of Texas at Austin
101 East 27th Street, Suite 4.300
Austin, TX 78712-1500
e-mail: pflerings@jsg.utexas.edu
Phone number: 512-475-9520

Prepared for:
United States Department of Energy
National Energy Technology Laboratory

January 23, 2014



Office of Fossil Energy



1 ACCOMPLISHMENTS:

1.1 *What are the major goals of the project?*

The project goal is to predict, given characteristic climate-induced temperature change scenarios, the conditions under which gas will be expelled from existing accumulations of gas hydrate into the shallow ocean or directly to the atmosphere. When those conditions are met, the fraction of the gas accumulation that escapes and the rate of escape shall be quantified. The predictions shall be applicable in Arctic regions and in gas hydrate systems at the up dip limit of the stability zone on continental margins. The behavior shall be explored in response to two warming scenarios: longer term change due to sea level rise (e.g. 20 thousand years) and shorter term due to atmospheric warming by anthropogenic forcing (decadal time scale).

Milestone Description	Planned Completion	Actual Completion	Verification Method	Comments (progress toward achieving milestone, explanation of deviation from plan, etc.)
1.A 1-D simulation of gas hydrate dissociation in natural systems.	9/30/2013	9/30/2013	Report	We have simulated hydrate dissociation due to temperature change with a fully coupled model and we are currently further exploring this behavior. Results presented in 12/1/2013 report (what was this called?)
1.B 1-D Simulation of gas hydrate dissociation in laboratory controlled conditions.	3/31/2014	11/1/2013	Report	We have performed numerical simulations to guide and design our experimental in July and August, 2013. We have also simulated behavior predicted for our next set of experiments currently ongoing.
1.C Model-based determination of conditions required for gas not to reach seafloor/atmosphere from dissociating hydrate accumulation.	3/31/2014	3/31/2014	Quarterly Report	We are currently addressing this for completion in March, 2014. A preliminary model has been constructed. Results presented in 12/1/2013 report and in this quarterly report.
1.D Determination of what hydrate reservoirs are at three-phase equilibrium.	12/30/2013	12/1/2013	Report	We developed an approach to characterize the in situ stability of hydrate reservoirs. We have applied the approach to known reservoirs. The results were presented in our 12/1/2013 report.
1.E Demonstrate ability to create and dissociate methane hydrate within sediment columns under conditions analogous to natural systems.	9/30/2013	10/15/2013	Report	We performed experiments in summer 2013 demonstrating the ability to create and dissociate hydrate three phase stability without adding the additional complexity of

				cooling from above or below. We are currently performing a second set of experiments.
2.A 1-D simulation of gas expulsion into hydrate stability zone.	9/29/2014		Report	Preliminary simulations produced
2.B Determination of conditions for which gas expulsion into hydrate-stability zone is self-limiting.	12/29/2014		Report	
2.C Demonstration of reaction transport experiment where gas invades hydrate stability zone and creates three phase stability.	9/30/2014		Quarterly Report	Currently developing/refining remote sensing technologies. Refining experimental design based on numerical simulation
2.D Demonstrate a 2D simulation of hydrate dissociation and gas expulsion.	3/31/2015		Report	

1.2 What was accomplished under these goals?

1.21 Task 1: Project Management and Planning:

In the last quarter, one post-doctoral scientist, and two graduate students worked on both experimental analysis and theoretical results. We now have 2 students and one post-doctoral scientist working full time on the project, in addition PI's Flemings and Bryant, Subcontractor Kneafsey, and lab scientist Peter Polito are working on the project. We have continued to have bi-monthly meetings with LBNL and between the Department of Geological Sciences and the Dept. of Petroleum and Geosystems Engineering. We also sent two of our scientists to work with LBNL on experimental results. Our focus over the quarter has been twofold: 1) design and perform our initial experiments and 2) continue one dimensional modeling at the lab and field scale simulating hydrate melting.

Considerable time was spent preparing our Continuation application which was submitted December 2013

1.22 Task 2: Conceptual and Numerical Model Development -1D:

Subtask 2.1 - Dissociation of 1D vertical hydrate accumulation

Subtask 2.2 - Apply 1D model to laboratory experiment

Subtask 2.3 - 1D models of natural examples

Subtask 2.3.1 Hydrate accumulations below permafrost

Subtask 2.3.2 - 1D model application to deposits near up-dip limit of stability zone on continental margins

Our progress under Task 2 is described below. We have developed a fully coupled 1D hydrate model. We have been performing simulations described in Subtask 2.1, 2.2, 2.3 and 2.3.2. These are described below and in the experimental section.

1.22a 1-D Warming simulations (Subtask 2.1, 2.3, 2.3.2)

The time evolution of the different cases is presented below as Figure 1. We have chosen to show a characteristic grouping of time slices to illustrate the basic difference in behaviors. The saturation profiles show two drastically different responses.

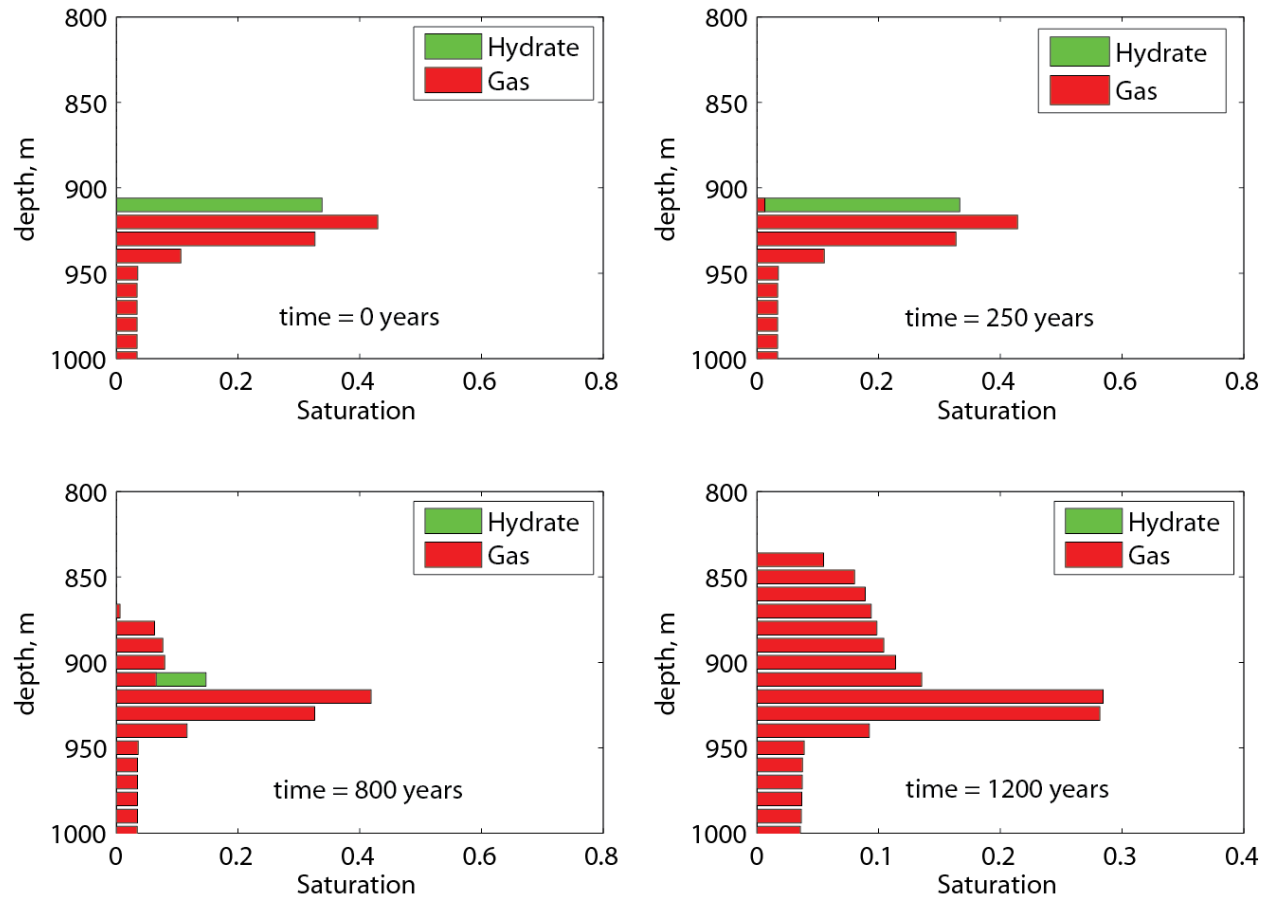


Figure 1: Gas and hydrate saturations versus depth at various stages of the dissociation process. Time increases L-R, then down. For the first 200 years, hydrate is still stable and warming has not propagated to the hydrate depth (upper left). At ~200 years, hydrate begins to dissociate and gas saturation increases locally. Between 200-1100 years, gas pressure increases and gas saturation exceeds the hydrate saturation (lower left). At ~1200 years, all hydrate has dissociated.

Case 1:

In Case 1, the hydrate at the base melts once the temperature perturbation has reached the BRHSZ. The bottom-most layer entirely dissociates, then the gas moves freely upward and reforms hydrate directly above, at the depth of the new RHSZ. During the dissociation of the hydrate, the warming signal ceases its propagation and the temperature at the dissociation depth is held fixed at the three-phase equilibrium temperature. Once the formation of hydrate begins, the latent heat of fusion introduces additional warming above and below the formation depth. The hydrate formation also increases the salinity due to the expulsion of salt in the hydrate structure. However, these effects are insufficient to alter the state of the system further. Instead, all of the methane that is mobile is converted to hydrate at its lowest possible depth. Once all of the mobile methane is re-converted to hydrate, the salt diffuses away from the source of the formation and the heat slowly diffuses away as well. The final hydrate deposit sits at the expected location and total methane losses are minimal and restricted to pressure

induced water flux into the ocean within the dissolved phase. The evolution of the profile as saturations v. depth plots and with temperature differences plots is presented in Figure 3 (while an example of the temperature difference plots is shown in Figure 2). The temperature difference plots illustrate the original quantity of warming provided by the seafloor perturbations in blue and the temperature required to reach three-phase equilibrium in red. A negative blue value indicates that seafloor forcing has not warmed the sediment at depth to its full potential. Additionally, a negative red value indicates that the sediment at depth is still within the L+H phase.

Case 2:

In Case 2, the hydrate at the base also melts once the temperature perturbation has propagated through the deposit. However, the upward migrating gas does not immediately reform hydrate. Instead, the overlying hydrate also undergoes dissociation and the free gas creates a pressure buildup. The pressure buildup forces gas migration. The gas at the new RHSZ does begin to reform some hydrate, but this additional heat and salinity is too much forcing for the overlying hydrate. These combined effects create a high salinity, high temperature pathway that ‘burns’ through the overly hydrate. Thus, a free gas pathway exists with venting into the ocean. This persists until the gas column loses its buoyancy driven mobility. Then, the top-most gas reforms hydrate capping additional free gas flow. The formation signal then propagates downward, depleting all of the available, mobile methane within the RHSZ. At the end of the simulation, there is a hydrate deposit situated where one would expect it to be based on a static, thermodynamic analysis. However, the dynamic adjustment drives ~25% of the original methane quantity (by volume) into the ocean. This evolution can most readily be seen by inspecting the panels in Figure 3b. At 2kyr, the three-phase distance has intersected the zero-threshold at a higher depth during the original dissociation. At 10 kyr, the entire deposit has crossed the three-phase threshold. Several thousand years are required before the deposit stabilizes into its new configuration.

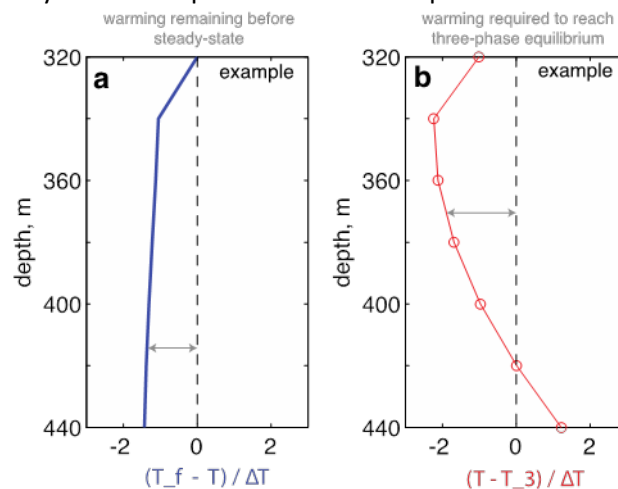


Figure 2: An example describing the plots to be presented in Figure 3. In these plots and the following plots, we emphasize the difference between the current temperature, T and some other important temperature. a) The difference between the current temperature, T , and the steady-state temperature achieved at infinite time. The difference is normalized by the temperature perturbation, ΔT . These plots will be presented in blue. b) The difference between the current temperature, T , and the temperature at three-phase equilibrium, given the current salinity and pressure. The difference is normalized by the temperature perturbation, ΔT . These plots will be presented in red with circles.

Salinity effects:

The general hydrate deposit evolution can be seen in Figure 4, which shows the salinity profiles at the same time slices as before. During dissociation, the salinity decreases due to the release of fresh water.

During formation, the salinity increases from the expulsion of salt in the hydrate structure. These salinity changes are largely responsible for the unique venting behavior shown in Case II. The hydrate stability temperature is a function of pressure and salinity, with lower salinity raising the stability temperature (increases the distance of the red curve), while increases in salinity lowers the stability temperature. In this way, the hydrate formation is a self-limiting process. With continued hydrate production, the pore-water will eventually become too saline and free gas will be stable in the presence of hydrate.

Venting:

We also show graphically how the gas venting varies over time in Figure 5. For Case I, no venting occurs, whatsoever. However, as previously discussed, there is a transient pulse of gas that vents into the ocean in Case II. This venting behavior is characterized by a sharp increase to a peak value followed by slightly less sharp decrease. This a pulse that dissipates and is not sustained throughout time. This behavior occurs over a ~5 kyr period.

Implications and Extensions

The simulation results presented show that for a given hydrate deposit there is a discrepancy between the static, thermodynamic analysis of macro-scale hydrate stability and the dynamic, fluid flow driven analysis of the same stability. In the latter analysis, there are methane losses into the ocean that are driven by the consequences of the phase changes. The volume expansion during hydrate dissociation drives gas flow upward, while the heat release and salinity increase during hydrate formation drives anomalous hydrate dissociation within the RHSZ.

These results are specific to the original parameters of the problem and clearly depend on the inherent 'distance' to the three-phase stability at the initiation of the simulation. Yet, we do not interpret this to be a faulty consequence of the model choices. Instead, it is this very 'distance', which we seek to quantify and explore. In previous studies of warming-induced hydrate dissociation, the deposits have been over-forced to cause complete hydrate depletion or have been warmed to cause shoaling of the RHSZ but at time scales too short to investigate the dynamic feedbacks of the phase changes. We contend that the 'switch' from venting-free RHSZ shoaling to venting from RHSZ shoaling is an important system change that informs the overall sensitivity of hydrate deposits to warming.

We plan to further explore this behavior in the coming months.

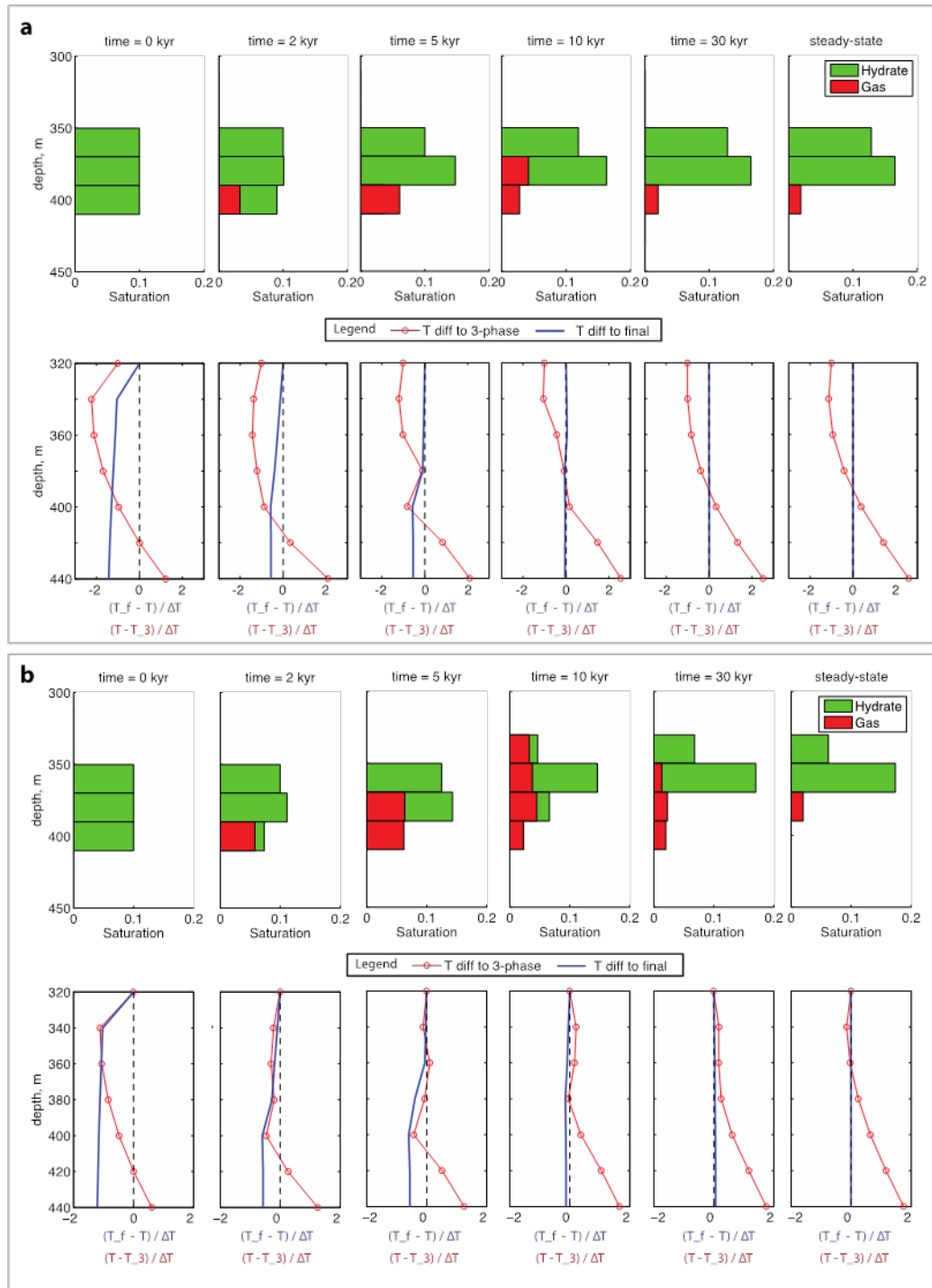


Figure 3: Time evolution of Case I and Case II. a) Case I Results, Top – The saturation profile for gas and hydrate. The gas is shown as red and the hydrate is shown as green. Initially there is 10% hydrate between depths 350m-410m. Bottom – The temperature evolution shown as differences. The temperature difference from the steady-state temperature is shown as the blue line. The temperature difference from the stability temperature is shown as the red line with open circles. See Fig. 2 for an example plot of these quantities. b) Case II results. All else is equal to (Fig. 3a).

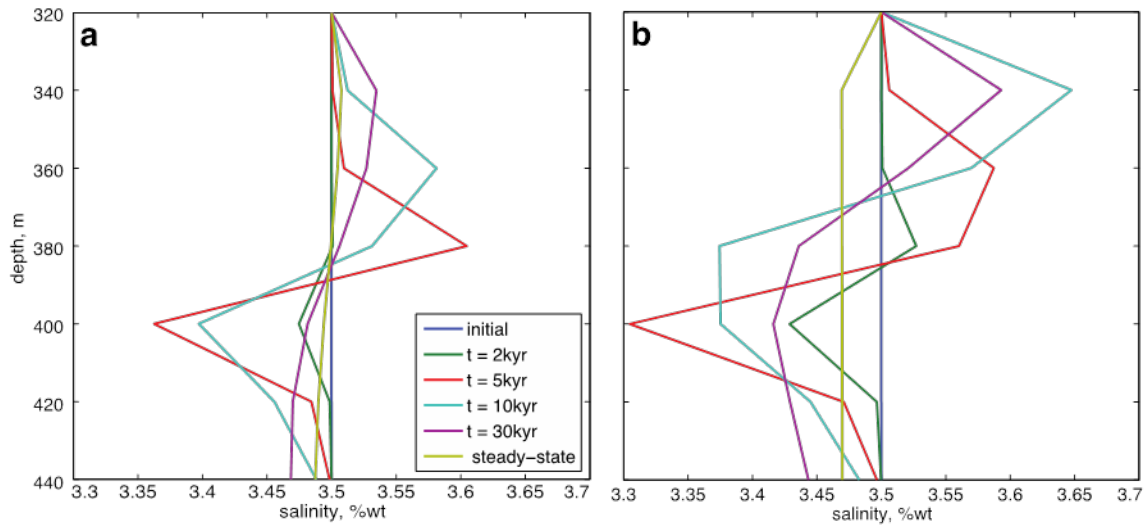


Figure 4: Evolution of the salinity profile in both cases. The time slices are the same time slices considered in Fig. 7a) Case I results. Note: The salinity profile has not equilibrated at the time of the temperature steady-state. b) Case II results.

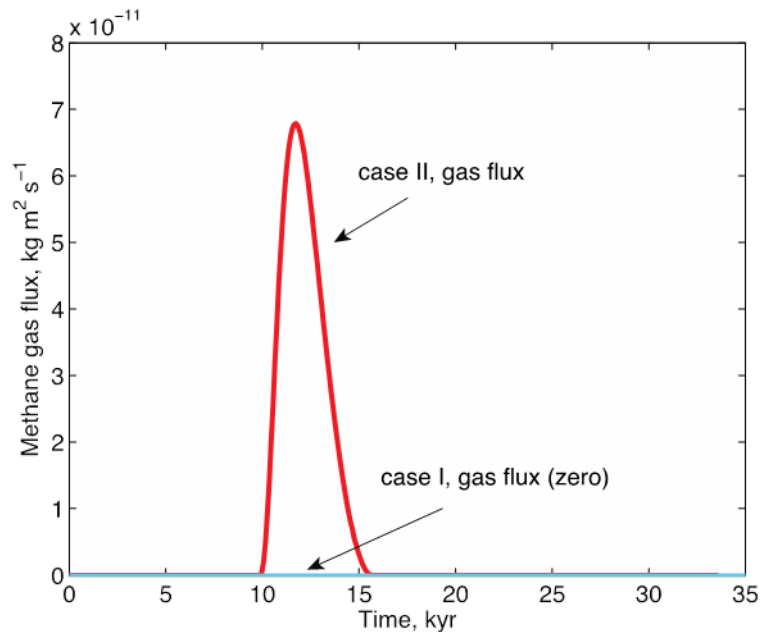


Figure 5: Gas flux venting into the ocean at the seafloor as a function of time. No gas flux for Case I. A transient pulse of gas flux for Case II lasting ~5 kyr.

1.22b Initial calculation for second step experiment (Subtask 2.2)

In the second round of experiments, we will form methane hydrate at three-phase equilibrium in a cylindrical sample chamber with 12.7 cm in length and 5.1 cm in diameter that is oriented vertically. We will use F-110 sand, which has a porosity of 36%, an intrinsic permeability of $8.3 \times 10^{-13} \text{ m}^2$, and capillary entry pressure of 0.02 MPa. We will initially saturate the sample with brine solution (NaCl). We will cool the sample homogeneously into the hydrate stability zone, and inject methane gas from the top or bottom of the sample at a constant rate.

To choose the values for the initial salinity, the experimental temperature and pressure condition and the gas injection rate, we developed a conceptual model of this experiment (Fig. 6) and a simplified analytical solution based on the assumptions of no long range transport of salt, local thermodynamic equilibrium, equal water and hydrate density, no water density change throughout the experiment and negligible amount of final gas saturations.

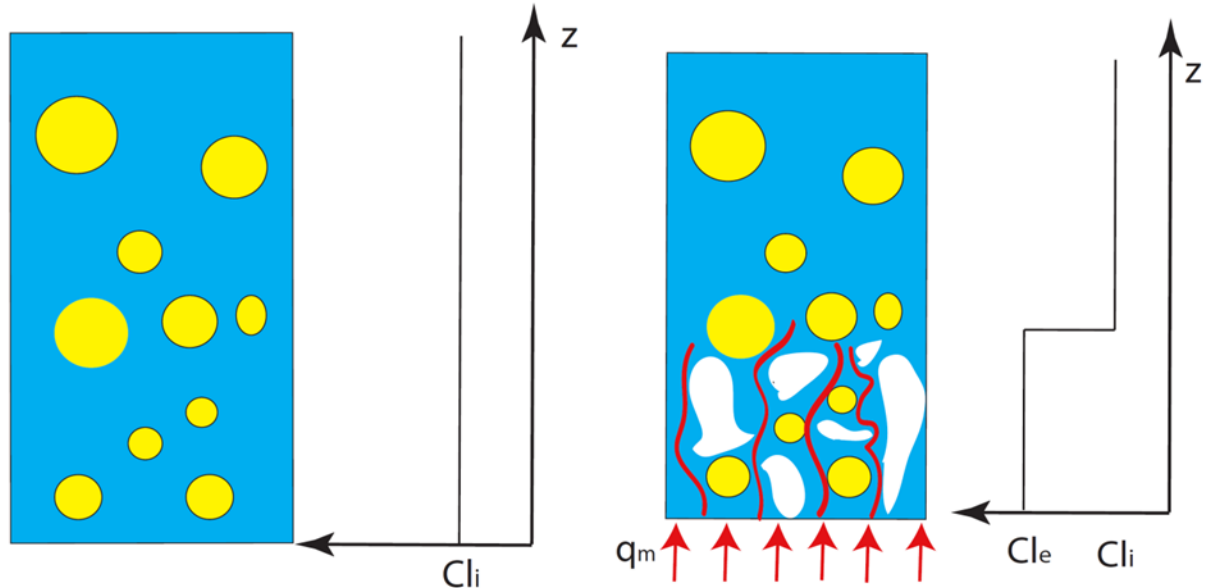


Figure 6: Conceptual model for hydrate formation at three phase equilibrium by injecting methane gas into a brine saturated sample with a constant rate. The sample is initially in hydrate stability zone (left figure). Behind the hydrate solidification front, the system is in three phase equilibrium condition (right figure). Cl_i is the initial salinity, Cl_e is the salinity at three phase equilibrium, q_m is the constant methane gas injection rate. The color of blue means water phase, white means hydrate phase, red means gas phase and yellow means solid grains.

Based on the mass conservation of salt, the hydrate saturation is calculated as

$$S_h = 1 - \frac{Cl_i}{Cl_e}, \quad \text{Eq. 1}$$

where S_h is the hydrate saturation at three phase equilibrium, Cl_i is the initial salinity (wt.%), Cl_e is the salinity at three phase equilibrium (wt.%).

The subcooling of the experiment is calculated as

$$\Delta T = T_e - T_{exp}, \quad \text{Eq. 2}$$

where ΔT is subcooling ($^{\circ}\text{C}$), T_e is the three phase equilibrium temperature at the initial pressure and salinity condition ($^{\circ}\text{C}$), T_{exp} is the experimental temperature ($^{\circ}\text{C}$).

The time for the whole sample to reach three phase equilibrium t_e (sec) is calculated as

$$t_e = \frac{L\phi S_h \rho_h M_m}{q_m M_h}, \quad \text{Eq. 3}$$

where L is the length of the sample (m), ϕ is the porosity of the sample, S_h is the hydrate saturation at three phase equilibrium, ρ_h is the methane hydrate density (912 kg m^{-3}), M_m is the methane molecular weight ($0.016 \text{ kg mol}^{-1}$), M_h is the methane hydrate molecular weight ($0.106 \text{ kg mol}^{-1}$), and q_m is the constant methane injection rate ($\text{kg m}^{-2} \text{ sec}^{-1}$).

Eqs. 1-3 are derived based on the assumption of no long range transport of salt or salt diffusion is negligible. For this assumption to be reasonable, the following relationship must be satisfied

$$q_m < \frac{D^m \phi S_h \rho_h M_m}{M_h L_{dif}}, \quad \text{Eq. 4}$$

where D^m is the salt effective diffusion coefficient in water phase in the sample ($\text{m}^2 \text{sec}^{-1}$), L_{dif} is the distance from the hydrate solidification front where salinity equals the initial value (m).

To choose the values for the initial salinity, the experimental temperature and pressure condition, we use the following criterion: first, the hydrate saturation at three phase equilibrium is less than 50% (so the intrinsic permeability of the sample will not be decreased dramatically); second, the experimental subcooling is as great as possible (to reduce the induction time of hydrate formation). Based on these criterions and using Eqs. (1)-(2), we choose the initial salinity of 7 wt.%, and experimental temperature of 2 °C and pressure of 7 MPa, which gives an experimental subcooling of 4.6 °C (Fig. 7).

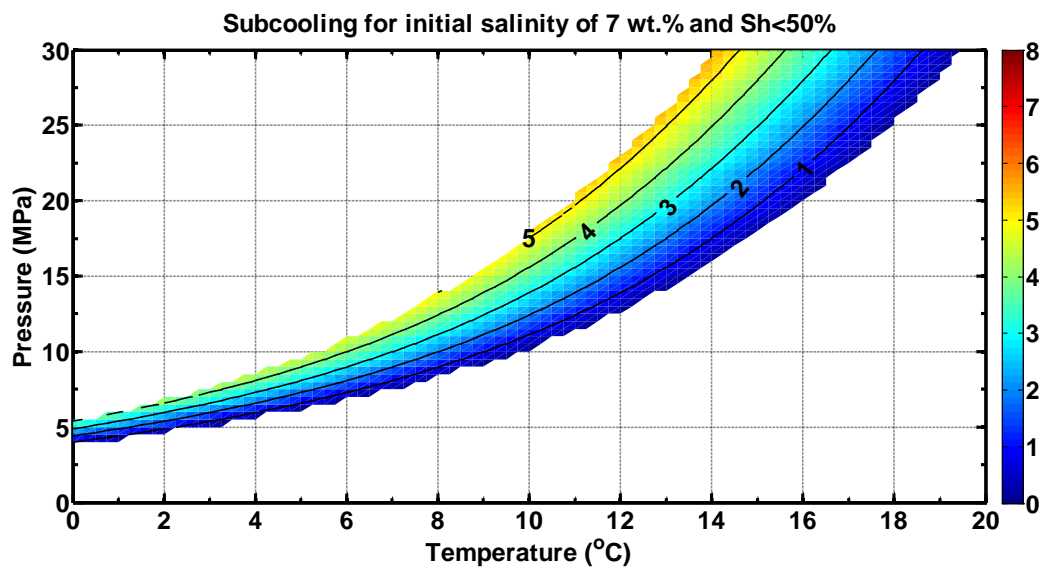


Figure 7: Subcooling for initial salinity of 7 wt.% with final hydrate saturation less than 50%. The pressure range is from 0 to 30 MPa, and the temperature range is from 0 to 20 °C. Lines with numbers are the contour lines for subcooling.

To choose the value for the methane gas injection rate, we use the following criterions: first, finish the experiment within predetermined amount of time; second, salt diffusion is negligible. Based on these criterions and using Eqs. (3)-(4), we choose the methane gas injection rate of $0.06 \text{ kg m}^{-2} \text{ hr}^{-1}$, which will allow the experiment to finish within 46 hours theoretically (Fig. 8).

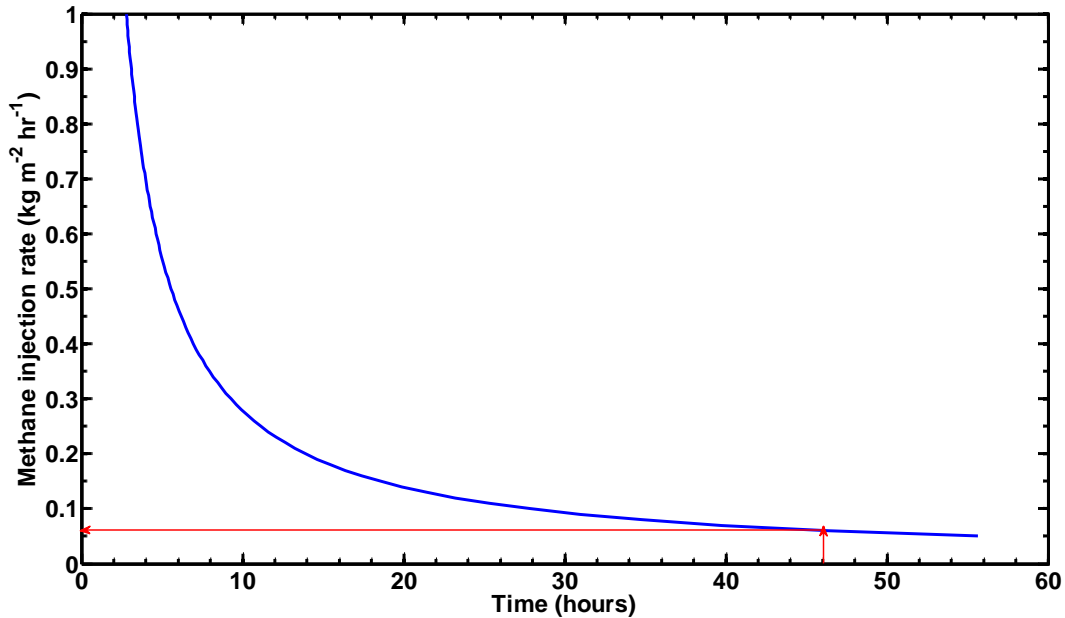


Figure 8: Methane gas injection rate versus time to fill a sample of 12.7 cm to three phase equilibrium. The sample has a porosity of 36%, pressure of 7 MPa and temperature of 2 °C. The sample is initially brine saturated with a salinity of 7 wt.%.

1.23 Task 3: Categorize stability of known hydrate reservoirs:

We examined the in-situ hydrate saturations and salinities of gas hydrate-bearing sediments at four sites on continental margins and in permafrost regions, to determine the thermodynamic state of each hydrate system. We determined hydrate saturations using logging-while-drilling (LWD) data in an iterative application of Archie's Law. The in-situ salinities were calculated from core-derived salinities by assuming that salts remained in the pore space, that the hydrate dissociated completely, and that pore volume remained constant with hydrate formation and dissociation. The in-situ salinity was compared to that required for three-phase equilibrium. We interpreted thick regions at three-phase equilibrium at three out of four of the study sites.

1.23a Determining in-situ hydrate saturation and salinity

We calculate the in-situ pressure and temperature by assuming constant geothermal and hydrostatic gradients. We use these values, in combination with the resistivity log, bulk density log, and core-derived salinity data to estimate the in situ hydrate saturation and salinity using the approach presented by Liu and Flemings (2006).

We assume only hydrate and water are present in the pore space, such that the volumetric pore saturation of hydrate (S_h) and water (S_w) are related by, $S_h = 1 - S_w$. We also assume that the pore volume and total in-situ salt mass and distribution do not change as a result of hydrate formation or dissociation. These assumptions are similar to those performed by Malinverno, et al. (2008). With these assumptions, we calculate the in-situ salinity ($C_{in-situ}$) with a volumetric correction between the core-derived salinity (C_0) and the water saturation:

$$C_{in-situ} = \frac{C_0}{1 - S_h} = \frac{C_0}{S_w} \quad \text{Eq. 5}$$

We determine the water saturation using Archie's Law (Archie 1941):

$$S_w = \frac{N \sqrt{a \cdot R_w}}{\phi^m \cdot R_t} \quad \text{Eq. 6}$$

where N is the saturation exponent, a is the tortuosity coefficient, R_w is the fluid resistivity, n is the porosity, m is the cementation exponent, and R_t is the formation resistivity. We use the RING resistivity from the LWD data as a reasonable estimate of the true formation resistivity (Cook et al. 2012). We calculate porosity using the bulk density log and the grain and fluid densities. We implement Arps' Equation (Arps 1953) to calculate the pore fluid resistivity.

Spangenberg (2001) showed that the N -value in modeled hydrate-bearing sediments increased to a maximum of 4 with increasing hydrate saturation. Since we are interested in regions with high hydrate saturations, we assumed that the saturation exponent was equal to 4 for these calculations.

We determine the tortuosity coefficient and cementation exponent for each site based on resistivity and porosity measurements where water is the only phase present ($S_w = 1$). With this assumption, Eq. 6 simplifies to:

$$F = \frac{R_t}{R_w} = a \cdot \phi^{-m} \quad \text{Eq. 7}$$

Where the formation factor (F) is the ratio of formation resistivity to fluid resistivity. A power law regression is taken from a cross-plot between porosity and formation factor and is used to infer the values of a and m . The porosity and resistivity data used in this method are filtered to ensure water-saturated points and good borehole conditions.

We used an iterative application of Archie's Law to determine the in-situ water saturation and salinity. This process uses the core-derived salinity to determine the initial fluid resistivity and then uses the corrected salinity from the previous iteration for the subsequent iteration. We found that the change in the calculated water saturation between iterations decreased significantly ($\Delta S_w < 1\%$) after 4 – 5 iterations.

During this process, two modes of linear interpolation were required to account for the different sampling resolutions of the log and core-derived data. The logged data resolution averaged 15.2cm (6in), while the core was sampled an average of every 493cm (194in). The first mode interpolated between the core-derived salinities to determine a unique salinity value for each resistivity data point, while the second mode interpolated between the resistivity measurements to determine a unique resistivity value for each salinity sample. Using these two interpolation methods, we produced hydrate saturation and salinity curves at both resolutions. These results are reported as gray or black lines for the resistivity resolution data and red dots for the salinity resolution data.

After determining the in-situ salinity and hydrate saturation, we calculated the salinity required for three-phase equilibrium for the interpreted temperature and pressure profiles at NGHP Site 01-10. This was accomplished using equilibrium solubility models defined by Duan, et al (1992) and Henry, et al (1999), as described by Liu and Flemings (2006).

1.23b Results

We present the in-situ hydrate saturations and salinities and interpret zones of three-phase equilibrium at four gas-hydrate bearing sites: a) ODP Site 1249A and Hydrate Ridge, offshore Oregon; b) IODP Site U1328A offshore Vancouver Island; c) NGHP Site 01-10A in the Krishna-Godavari Basin, offshore India; d) Mallik Site 5L-38 in the Mackenzie Delta, Northwest Territories, Canada.

ODP Site 1249A

ODP Site 1249A (Fig. 9) was drilled on the southern summit of Hydrate Ridge, offshore Oregon ($44^{\circ} 34.237'N$, $125^{\circ} 8.841'W$) in a water depth of 788.5 m to a total depth of 90 meters below seafloor (mbsf). The BSR occurred at approximately 115 mbsf. The stratigraphy at this site consists primarily of silty-clay with interbedded sandy layers. The presence of gas hydrate was confirmed through the occurrence of soupy or “mousse-like” textured sediments, caused by hydrate dissociation, and from whole-round cores where hydrate samples were preserved (Shipboard Scientific Party 2003). The standard suite of LWD instruments were deployed throughout the cored section of the well. Archie’s parameters, a and m , were determined to equal 1.50 and 1.89, respectively.

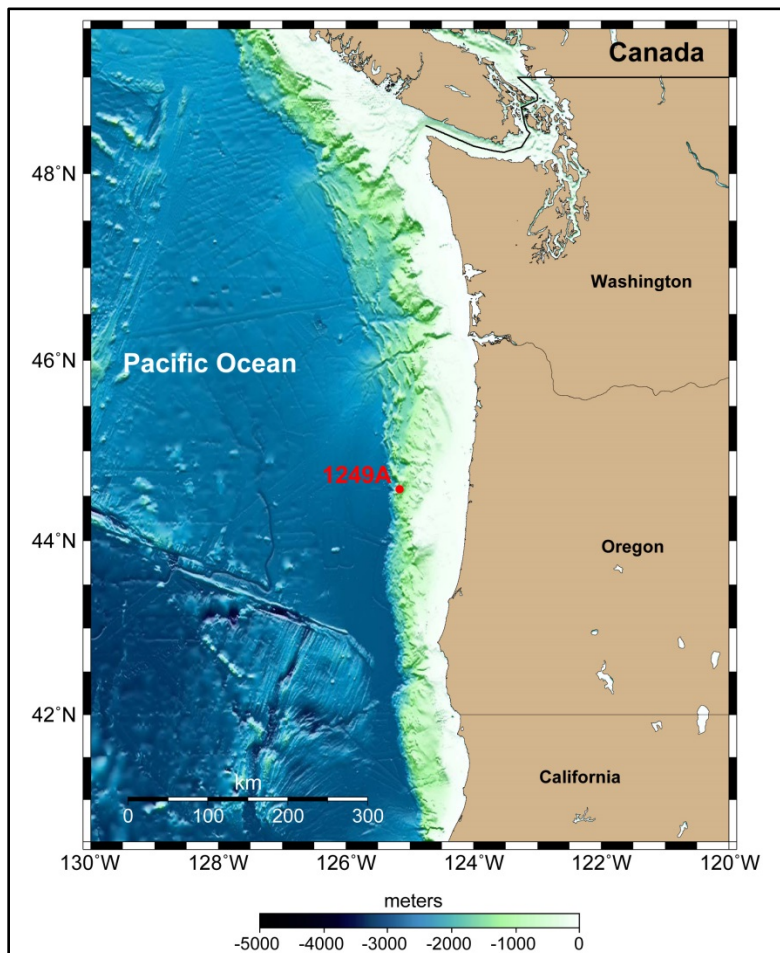


Figure 9: ODP Site 1249A is located approximately 90km offshore Oregon in about 790m of water. Bathymetry data from IOC, et al. (2003).

We identify existing regions of high in-situ hydrate saturations between 6 – 52 mbsf, decreasing significantly toward the base of the GHSZ (Fig. 10; Track 1). These zones of high hydrate saturation are

DOE Award No.: DE-FE0010406

DUNS No.: 170230239

Quarterly Research Performance Progress Report (Period ending 12/31/2013)

CONTROLS ON METHANE EXPULSION DURING MELTING OF NATURAL GAS HYDRATE SYSTEMS: TOPIC AREA 2

correlated with zones where the in-situ salinities are near to or exceed the salinity required for three-phase equilibrium, decreasing to just above seawater values near the base of the GHSZ (Fig. 10; Track 2). The in-situ salinity we calculated at 14 mbsf correlates well with the value determined from a pressure core sample taken at this sample depth (Milkov et al. 2004). These results suggest that three-phase equilibrium exists between 6 – 52 mbsf at this site.

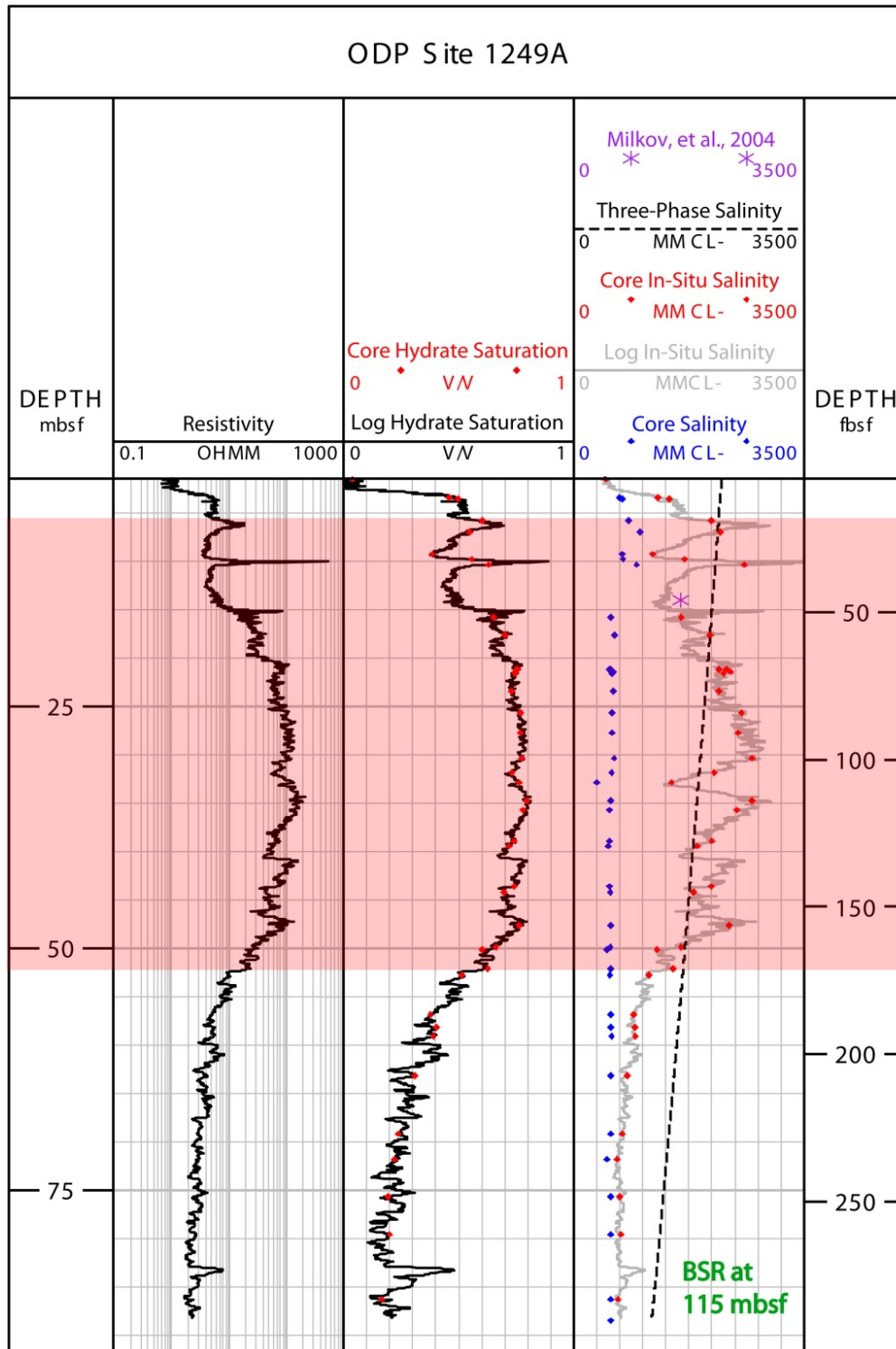


Figure 10: Results from ODP Site 1249A. Track 1: LWD resistivity; Track 2: Resistivity (black line) and salinity (red dots) interpolated, Archie-derived hydrate saturation; Track 3: Core-derived salinity (Shipboard Scientific Party 2003), resistivity (grey line) and salinity (red dots) interpolated in-situ salinities, in-situ salinity determined from a pressure core, and the salinity required for three-phase equilibrium (dashed line). Red box shows qualitatively interpreted three-phase equilibrium zone.

IODP Site U1328A

IODP Site U1328A (Fig. 11) was drilled on the mid-continental slope off of Vancouver Island ($38^{\circ} 40.057'N$, $126^{\circ} 51.043'W$) in a water depth of 1267.7 m to a total depth of 300 mbsf, penetrating the base of the GHSZ at 219 mbsf. The stratigraphy in this region is dominated by silty-clay with interbedded coarser-grained material. The presence of gas hydrate was confirmed through infrared temperature data as well as the incidence of soupy or “mousse-like” textured sediment caused by hydrate dissociation (Expedition 311 Scientists 2006). The standard suite of LWD instruments were deployed throughout the cored section of the well. Archie’s parameters, a and m , were determined to equal 1.48 and 1.40, respectively.

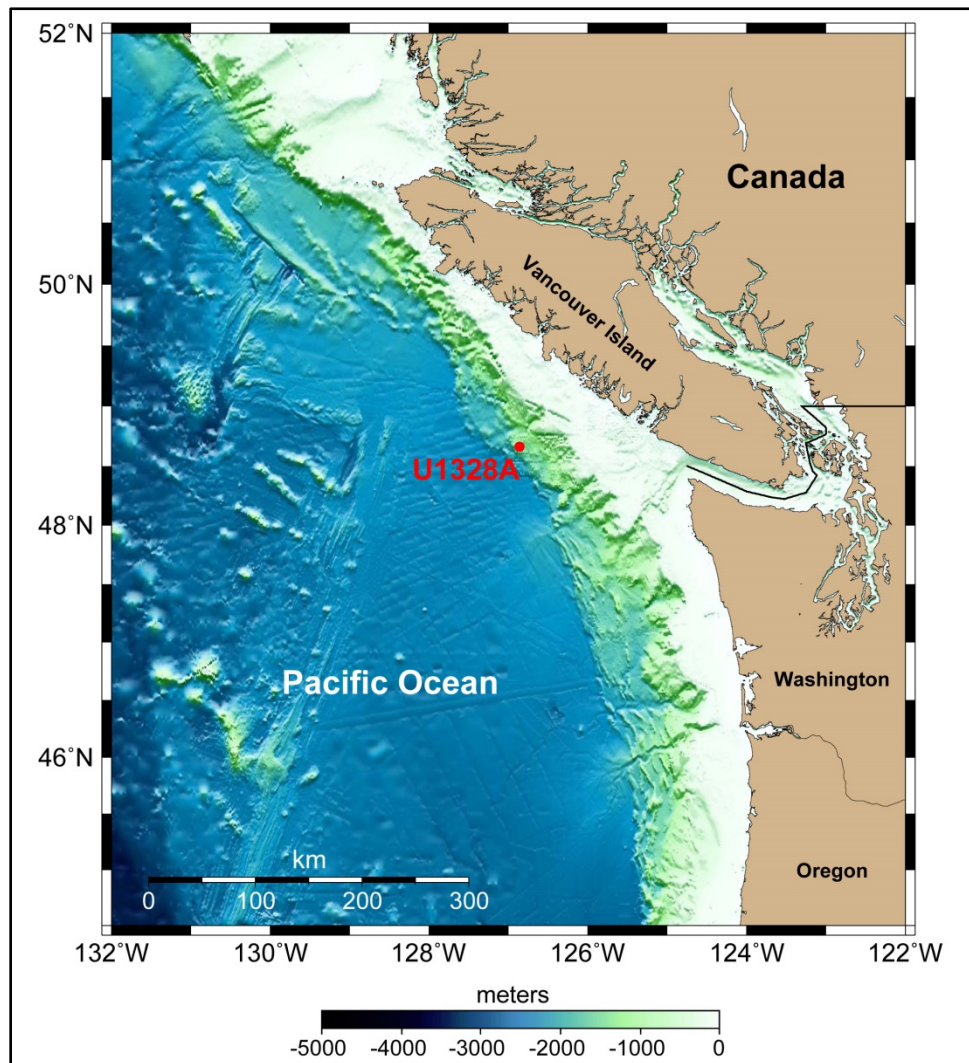


Figure 11: IODP Site U1328A is located approximately 100km offshore Vancouver Island in about 1270m of water. Bathymetry data from IOC, et al. (2003).

We identify a relatively thin region of the GHSZ (0 – 30 mbsf) with high hydrate saturation, which decreases rapidly to essentially no hydrate for the rest of the GHSZ (Fig. 12; Track 1). This zone of high hydrate saturation is correlated with elevated salinities near the top of the GHSZ, but do not reach the three-phase boundary (Fig. 12; Track 2). These results suggest that no portion of this system is at three-phase equilibrium.

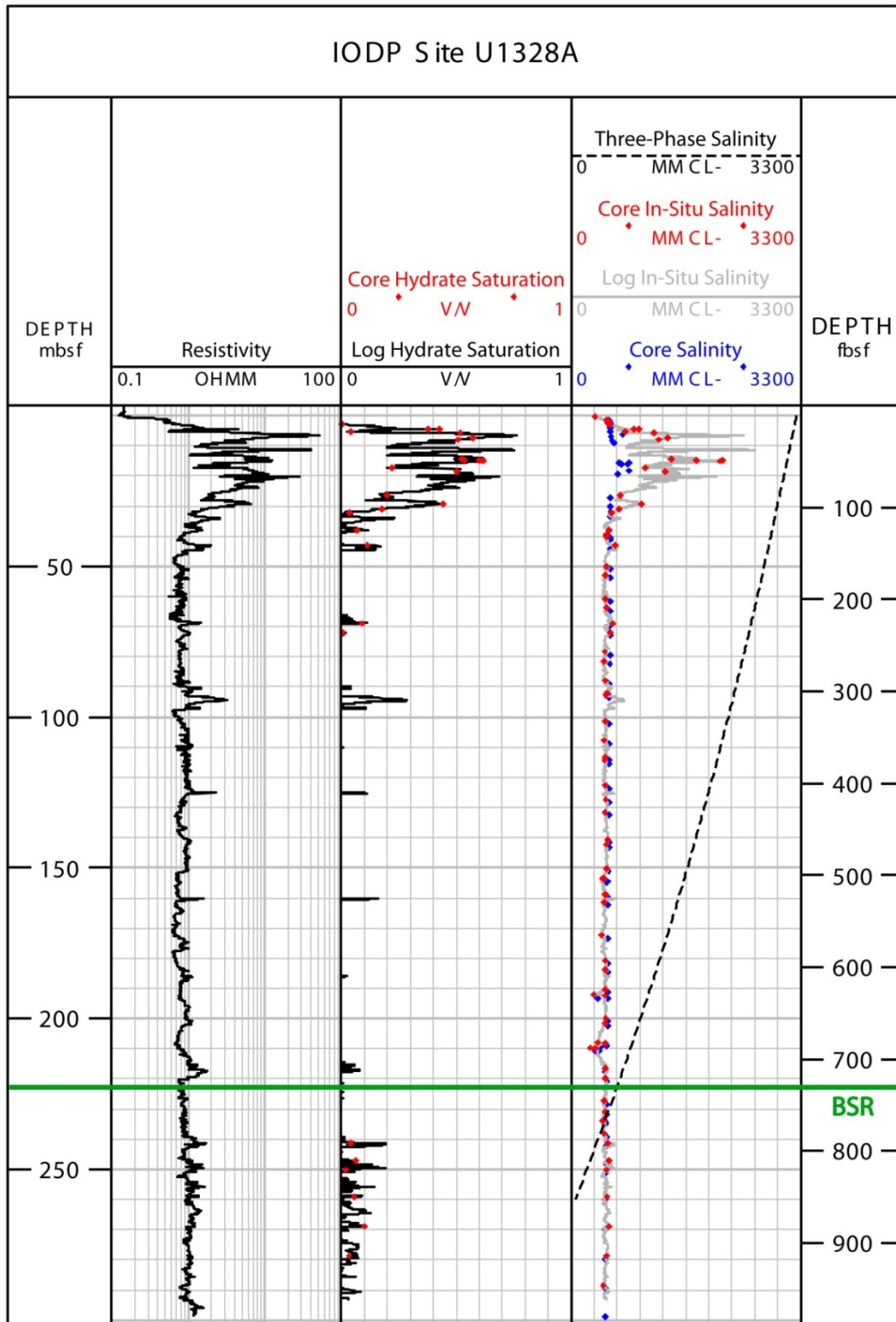


Figure 12: Results from IODP Site U1328A. Track 1: LWD resistivity; Track 2: Resistivity (black line) and salinity (red dots) interpolated, Archie-derived hydrate saturation; Track 3: Core-derived salinity (Expedition 311 Scientists 2006), resistivity (grey line) and salinity (red dots) interpolated in-situ salinities, and the salinity required for three-phase equilibrium (dashed line).

NGHP Site 01-10A

NGHP Site 01-10A (Fig. 13) was drilled in the Krishna-Godavari Basin, off the eastern coast of India ($15^{\circ} 51.857'N$, $81^{\circ} 50.079'E$). The site was drilled in a water depth of 1049.4 m to a total depth of 205 mbsf, penetrating the base of the GHSZ at 160 mbsf. The stratigraphy at this site is dominated by clay with interbedded silty and carbonate rich layers. The presence of hydrate was confirmed in core sample cuts, IR data, and the occurrence of soupy or “mousse like” textured sediment as a result of hydrate dissociation. The hydrate observed was found in three, void-filling structures: a) solid nodules, b) high-angle fracture-filling veins, and c) disseminated within the pore space (NGHP Expedition 01 Scientists 2007). The standard suite of LWD instruments were deployed throughout the cored section of the well, however, some logging data was unavailable above 30 mbsf. Archie’s parameters, a and m , were determined to equal 1.5 and 1.75, respectively.

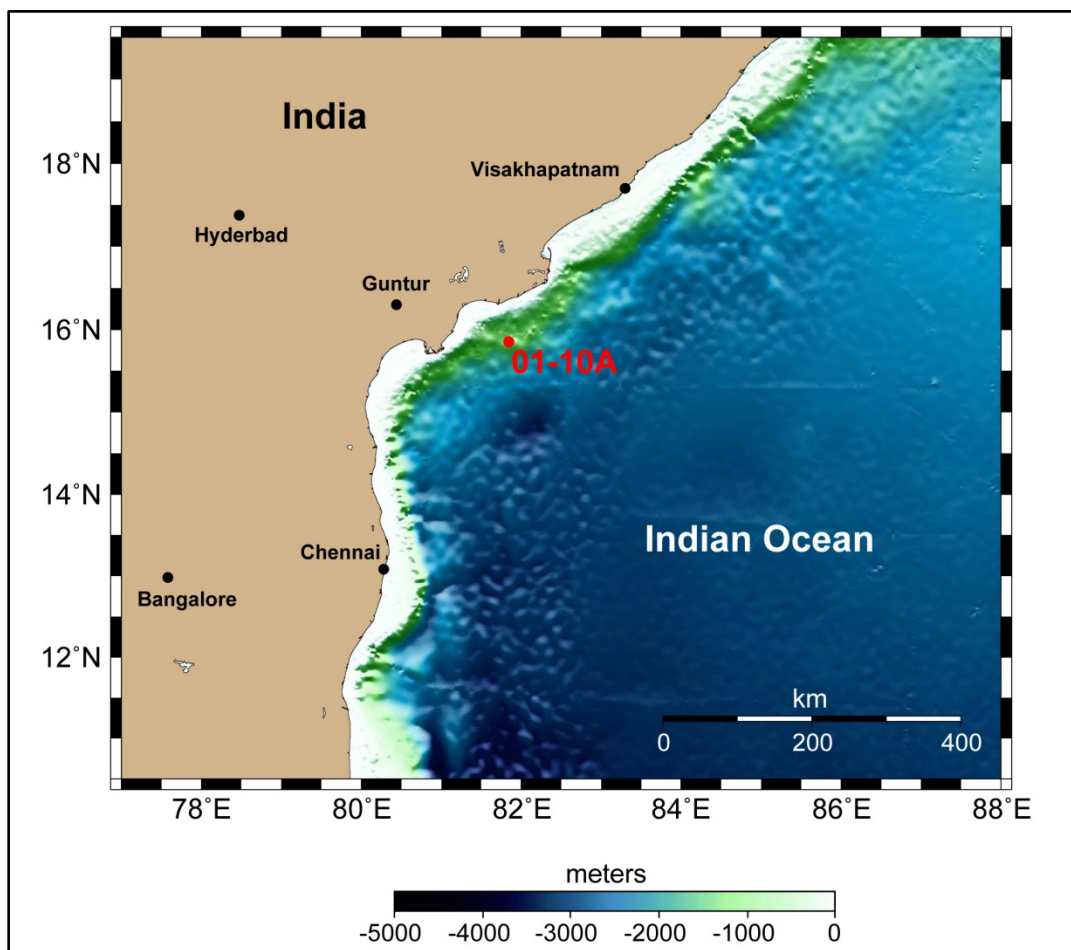


Figure 13: NGHP Site 01-10A is located approximately 60km offshore the eastern coast of India in about 1050m of water. Bathymetry data from IOC, et al. (2003).

We identify two thick regions of high in-situ hydrate saturations within the GHSZ from 45 – 90 and 123 – 160 mbsf (Fig. 14; Track 1). These zones of high hydrate saturation are correlated with elevated in-situ salinities near to or exceeding the salinity required for three-phase equilibrium (Fig. 14; Track 2). These results suggest that these two zones of this reservoir are at three-phase equilibrium.

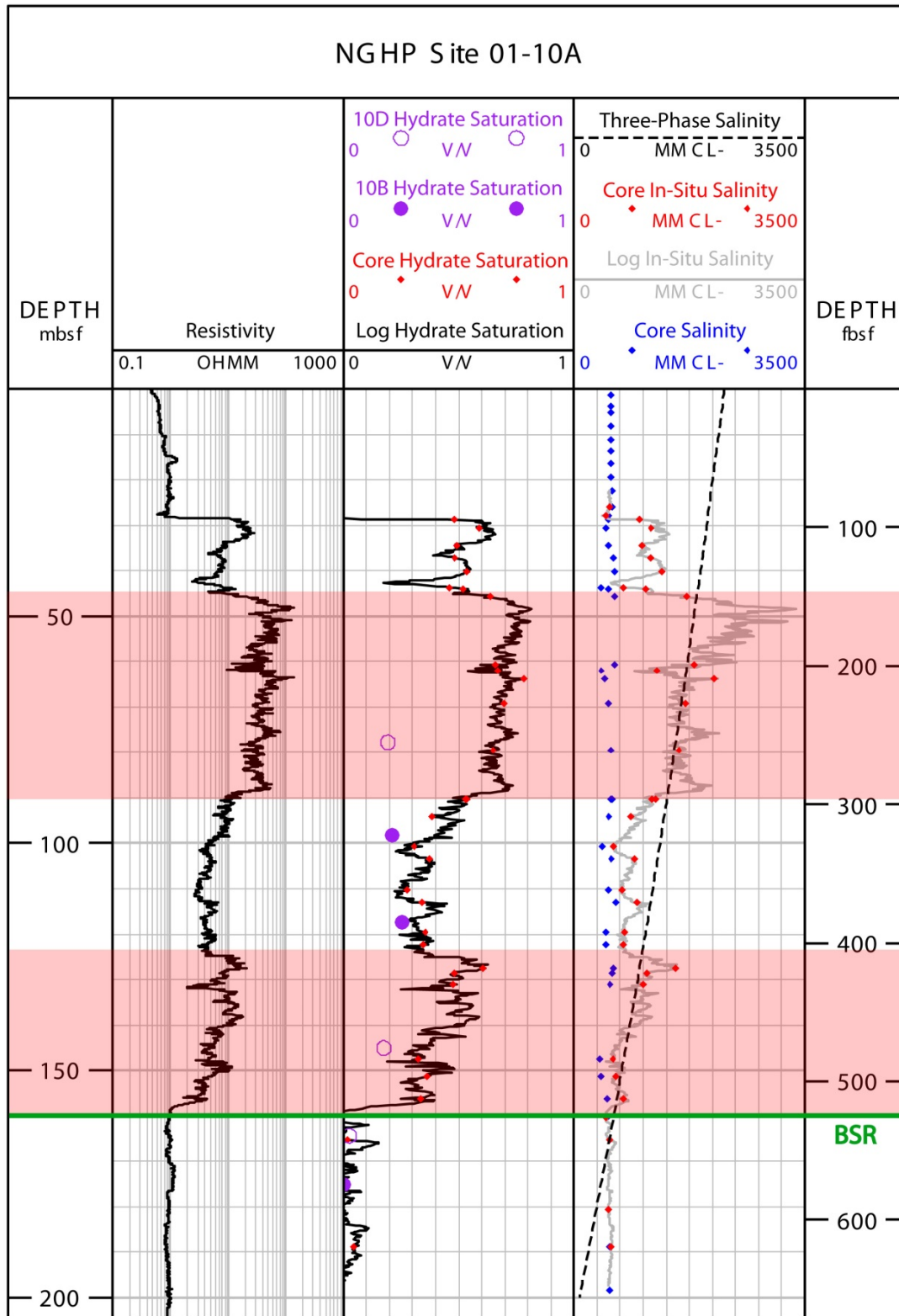


Figure 14: Results from NGHP Site 01-10A. Track 1: LWD resistivity; Track 2: Resistivity (black line) and salinity (red dots) interpolated, Archie-derived hydrate saturation and the hydrate saturation calculated from pressure cores recovered from Site-01-10B and 01-10D (NGHP Expedition 01 Scientists 2007); Track 3: Core-derived salinity (NGHP Expedition 01 Scientists 2007), resistivity (grey line) and salinity (red dots) interpolated in-situ salinities, and the salinity required for three-phase equilibrium (dashed line). Red boxes show qualitatively interpreted three-phase equilibrium zones.

Mallik Site 5L-38

Mallik Site 5L-38 (Fig. 15) was drilled in the Mackenzie River Delta in the Northwestern Territories, Canada (69° 27.655'N, 134 ° 39.648'W). The site was drilled in a water depth of 1 m to a total depth of 1166 mbsf. The upper 676.5 mbsf consists of permafrost-cemented sediment, underlain by water saturated sediment in which hydrate formed between 891 and 1107 mbsf (Collett, Lewis and Dallimore 2005, Takahashi, Fercho and Dallimore 2005). The stratigraphy within the GHSZ consists of 4 thick layers of sandy material separated by thick, fine-grained silt layers (Medioli et al. 2005). The presence of gas hydrate in the area was previously confirmed in 1972 and 1998 (Bily and Dick 1974, Collett and Dallimore 1998, Dallimore, Uchida and Collett 1999) during the drilling of the Mallik L-38 and 2L-38 wells, respectively, and was also confirmed at the 5L-38 well through the presence of hydrate in recovered cores and use of pressure core samples to specifically recover hydrate samples (Lu et al. 2005). This well was divided up into 4 distinct zones based upon the core-derived chloride concentrations in Matsumoto, et al. (2005) and supported by the lithology in that same study. There was an extensive wireline logging program implemented within the GHSZ at this site. Archie's parameters, a and m , were determined to equal 0.75 and 2.05, respectively.

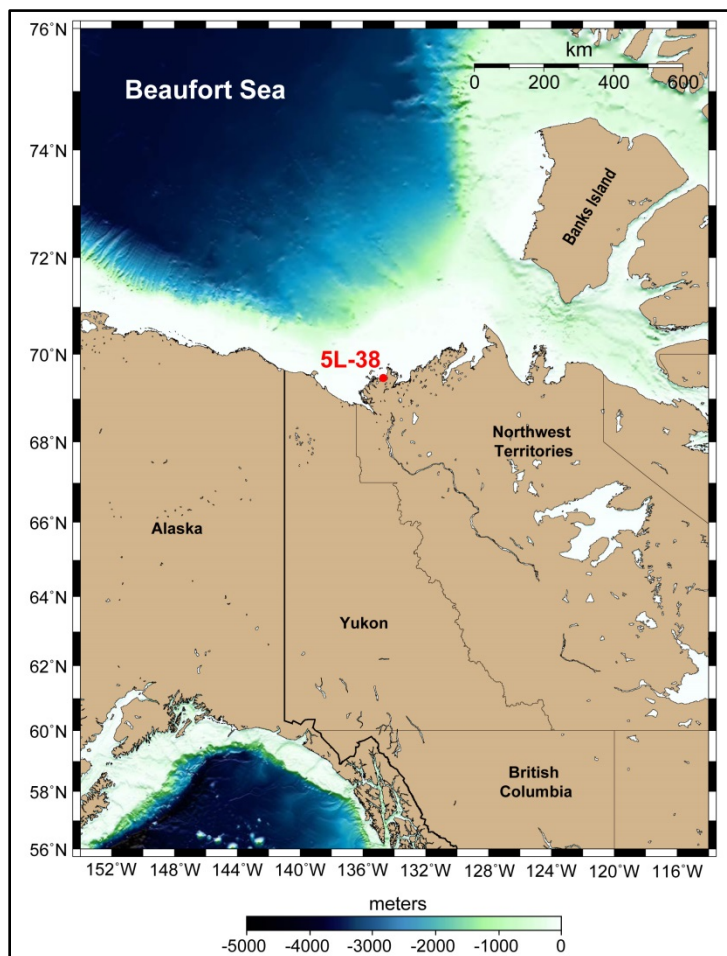


Figure 15: Mallik Site 5L-38 is located in the Mackenzie River Delta in 1m of water. Bathymetry data from IOC, et al. (2003).

Hydrate formation at Mallik 5L-38 is limited to Zone 3, with decreasing hydrate saturation towards the seafloor (Fig. 16; Track 1). Our calculated hydrate saturations correlate well with the saturations determined from the pressure core sampling program (Lu et al. 2005). This zone of high saturation is

DOE Award No.: DE-FE0010406

DUNS No.: 170230239

Quarterly Research Performance Progress Report (Period ending 12/31/2013)

CONTROLS ON METHANE EXPULSION DURING MELTING OF NATURAL GAS HYDRATE SYSTEMS: TOPIC AREA 2

associated with elevated in-situ salinities that approach or cross the three-phase boundary (Fig. 16; Track 2). From these results, we interpret three-phase equilibrium zones between 1060 – 1107 mbsf.

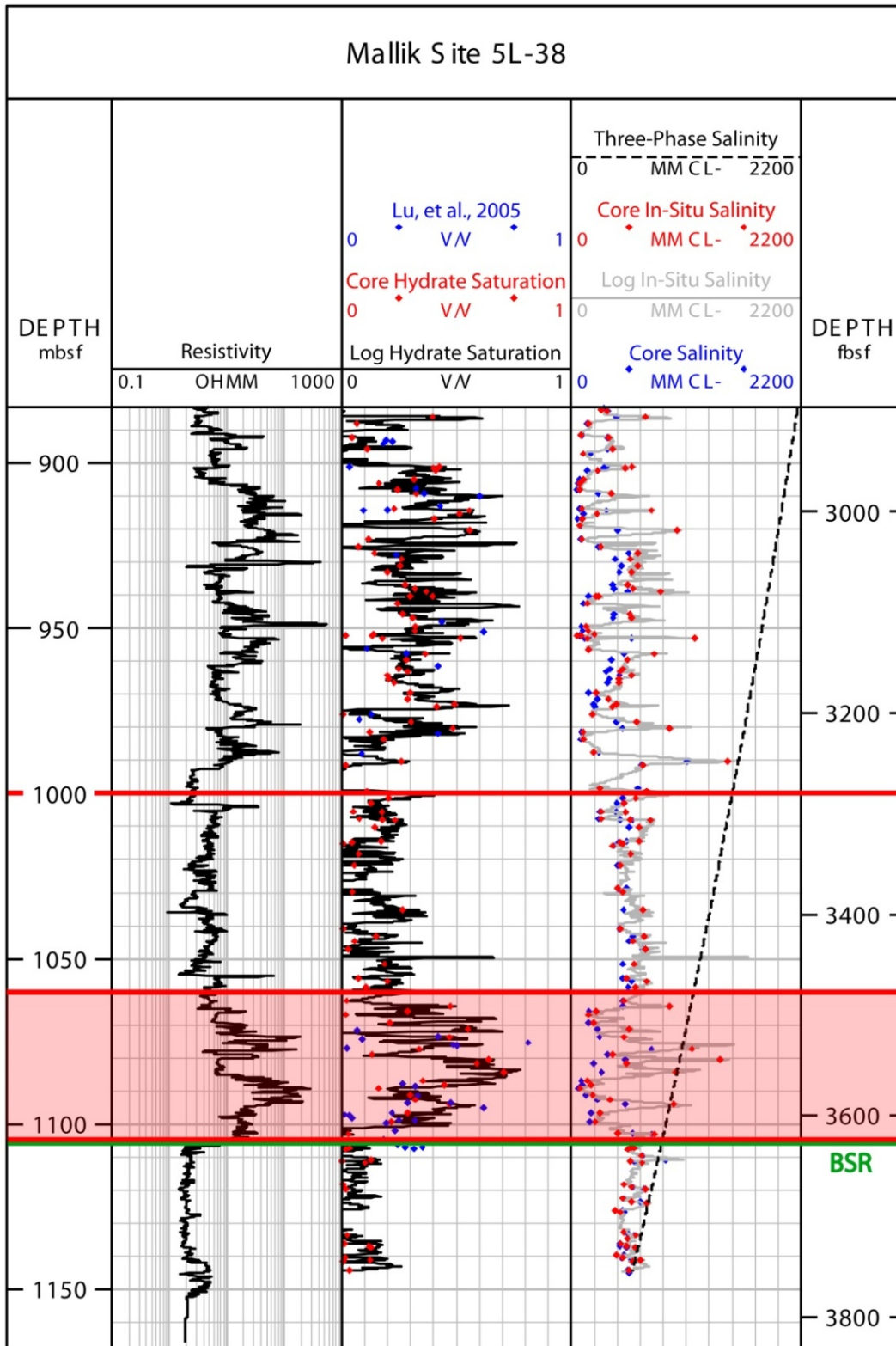


Figure 16: Results from Mallik Site 5L-38. Track 1: LWD resistivity; Track 2: Resistivity (black line) and salinity (red dots) interpolated, Archie-derived hydrate saturation and the hydrate saturations reported by Lu, et al. (2005) from pressure cores; Track 3: Core-derived salinity (Matsumoto et al. 2005), resistivity (grey line) and salinity (red dots) interpolated in-situ salinities, and the salinity required for three-phase equilibrium (dashed line). Red box shows qualitatively interpreted three-phase equilibrium zone.

1.23c Discussion

We present the in-situ hydrate saturation and salinity of four different hydrate-bearing sites. At ODP Site 1249A, we document a region between 6 – 52 mbsf with elevated in-situ salinities near the three-phase boundary. The lateral migration of gas from below ODP Site 1250 to Site 1249A within the GHSZ has limited hydrate formation to the upper portion of the GHSZ below Site 1249A (Liu and Flemings 2006, Milkov et al. 2004) and caused the observed hydrate saturation and salinity profiles. At IODP Site U1328A, we document that elevated salinities only exist in the upper 30 mbsf and are not near the three-phase boundary. The concentration of hydrate near the seafloor is produced as a result of the sedimentation and dissolved methane advection rates (Malinverno et al. 2008). At NGHP Site 01-10A, we document elevated salinities near the three-phase boundary in two thick zones within the GHSZ, separated by a thick two-phase (L+H) region. The lithology of this site shows that the two-phase region is associated with large amounts of authigenic carbonate and carbonate cement, while the three-phase regions are relatively clear of carbonates (NGHP Expedition 01 Scientists 2007), suggesting that hydrate formation in this region is limited by the carbonate lithology. Finally, at Mallik Site 5L-38, although we identified high hydrate saturation and three-phase equilibrium in Zone 3. The distribution of hydrate within this reservoir seems to be controlled by the dominant lithology, with hydrate formation concentrated in coarse-grained layers and limited in fine-grained layers (Matsumoto et al. 2005). These results indicate that significant portions of the reservoirs at ODP Site 1249A, NGHP Site 01-10A, and Mallik Site 5L-38 are at or near three-phase equilibrium, while IODP Site U1328A is not at three phase equilibrium. Reservoirs that are at three-phase equilibrium require only small fluctuations in in-situ conditions to cause hydrate dissociation and are therefore less stable than those reservoirs not at three-phase equilibrium. From this, we conclude that large portions of many of the sites studied here are thermodynamically unstable.

1.24 Task 4: Laboratory Evaluation of Hydrate Dissociation:

Subtask 4.1 - Freezing to 3 phase stability conditions, followed by melting from above

Subtask 4.2 - Freezing to L+H condition, warming from above

Subtask 4.3 - Freezing to L+H condition, warming from below

Our experimental work has been focused on two fronts: i) completing an analysis on our initial set of experiments performed in summer 2013; and ii) initiating a second set of experiments. We report on each of these below.

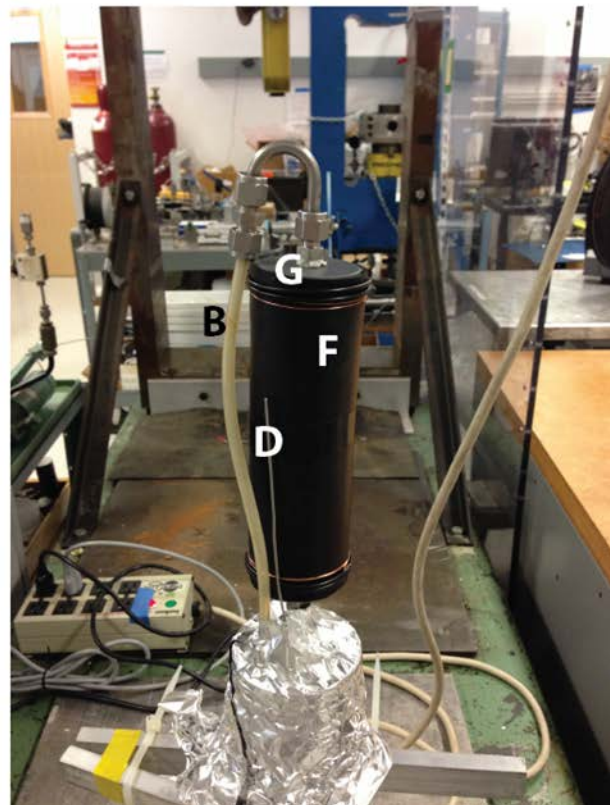
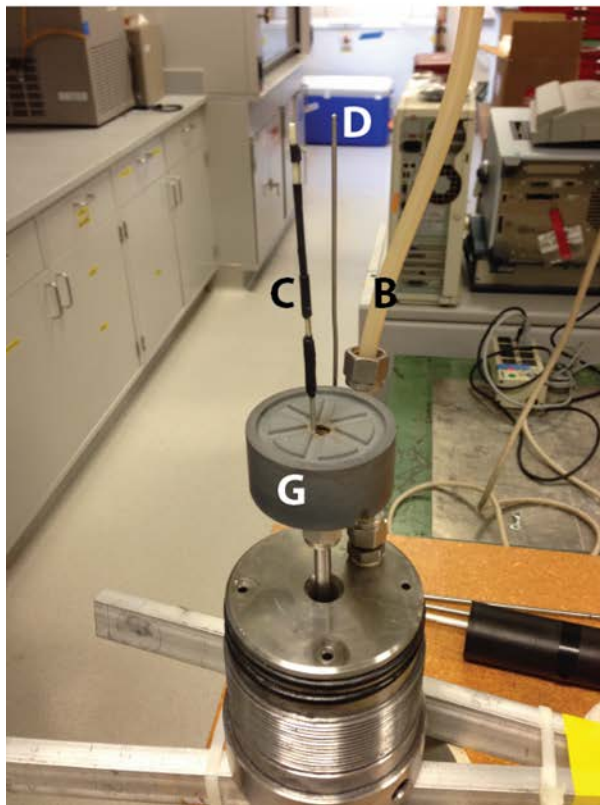
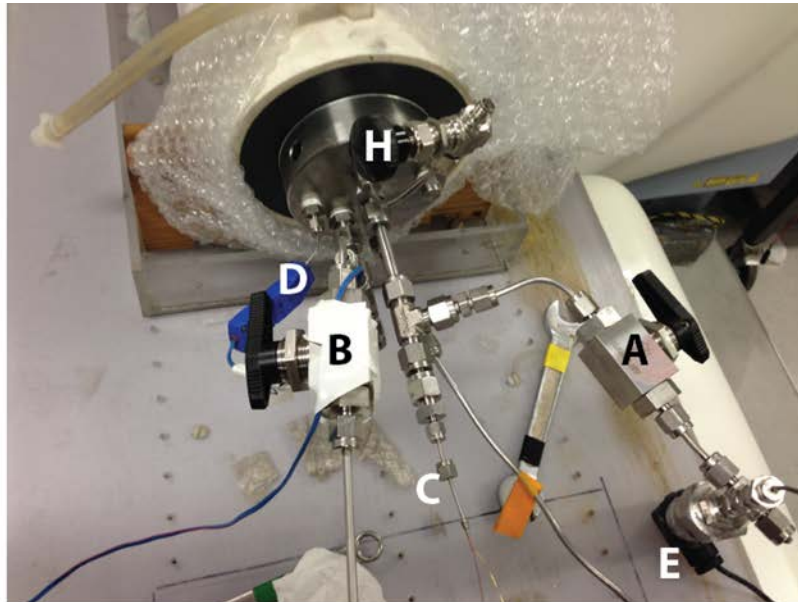


Figure 17: Experimental system. The pertinent components of this system are the a) pore pressure inlet, b) pore pressure outlet, c) resistivity array, d) thermocouple, e) pore pressure sensor, f) EPDM sleeve (encasing the sample), g) end caps, and h) cell pressure inlet/outlet.

1.24a Experimental results

We have made considerable progress analyzing our data from our first experiment. One of the most significant steps forward was to quantify the amount of hydrate present in the vessel throughout the

experiment. We review these advances here.

Further analysis of summer 2013 experiment:

In addition to monitoring temperature, pressure, and electrical resistivity, the test was monitored using a GE Lightspeed 16 X-ray CT scanner providing spatially resolved density information. The average density change from the initial condition of each of the 204 slices (0.625 mm in thickness) for a single scan is plotted in Fig. 18(a). As methane hydrate started to form after Day 7.4, the bulk density on the left side (downstream from the inlet) increased while that on the right side (upstream) decreased. The zone with increased density gradually became smaller and denser toward the middle of the left half sample from Day 8.7 to Day 15.4 (Fig. 18(a)). From Day 19.4 to Day 25.4, the temperature was stepwise increased and the bulk density change gradually returned to about zero across the sample.

Fig. 18(b) shows the average bulk density of each of the 204 slices at the initial pressure and temperature when the sample was filled with 49 vol.% brine and 51 vol.% methane gas, when the sample was saturated with brine, when the sample was saturated with fresh water and when the sample was dry and saturated with nitrogen. The average bulk densities at these conditions from 10 mm to 105 mm were 1.898, 2.028, 2.020 and 1.750 g cm⁻³, respectively. We took the average bulk density from 10 mm to 105 mm because the data from 0 to 10 mm and from 105 to 127 mm were not reliable. This is because the packing was different at downstream end (left end) because inserting the endcap inevitably disturbed the sample there (packing was conducted from upstream end to downstream end); second, sand flowed out of the sample at the upstream end (right end) upon injection of brine after hydrate dissociation. The grain density, density of brine with 3.5 wt.% salinity and fresh water density were 2.65, 1.030 and 1.002 g cm⁻³ at pressure of 6.94 MPa and temperature of 17 °C, respectively. Gas density is negligible compared with other density values (about 0.053 g cm⁻³ for methane at 6.94 MPa and 17 °C).

Seol and Kneafsey (2011) provided the following equations to calculate the saturations based on the assumptions of negligible gas density, constant water to methane molecular ratio of 5.75 in methane hydrate, methane hydrate density of 0.912 g cm⁻³, no movement of sand grains and no change of brine density during the experiment.

$$S_T = \frac{CT_e - CT_{\text{dry}}}{CT_{\text{sat}} - CT_{\text{dry}}}. \quad \text{Eq. 8}$$

where CT_{dry} and CT_{sat} are the bulk density (kg m⁻³) from CT scans at the dry and brine saturated conditions. CT_e is the bulk density at the condition to be estimated (kg m⁻³). S_T is the total saturation of water and hydrate on the water basis in presence of hydrate, which is equal to water saturation if there is no hydrate. Water saturation (S_w) and hydrate saturation (S_h) in the system in presence of gas hydrate are computed using the equations:

$$S_w = \frac{S_T}{\left(1 + \frac{Xf}{1-X}\right)}, \quad \text{Eq. 9}$$

$$S_h = \frac{S_T \rho_w / \rho_h}{\left(1 + \frac{1-X}{Xf}\right)}, \quad \text{Eq. 10}$$

where ρ_w and ρ_h are the water and hydrate phase densities (kg m^{-3}), respectively, f is the mass ratio of the hydrate to the initial water in methane hydrate and $f=1.15$, and X is the fraction of initial water converted into hydrate. X can be calculated using the measured methane mass consumption divided by the total methane mass required to transform all the water in the system to hydrate (7.8 g in this study). The same X is assumed to apply to all slices in this study. If X is overestimated, S_w is underestimated, and S_h is overestimated. Detailed information about this method can be found in Seol and Kneafsey (2011).

Using Eq. 8 and the average bulk densities of 1.898, 2.028 and 1.750 g cm^{-3} at the initial, brine saturated and dry conditions (Fig. 18(b)), we obtained the initial water saturation of 53 vol.%, which was close to the actual initial water saturation of 49 vol.%. In addition, using these average bulk densities in Fig.18(b) and the densities of grain (2.65 g cm^{-3}), initial brine (1.030 g cm^{-3}), fresh water (1.002 g cm^{-3}) and the estimated initial water saturation of 53 vol.%, we obtained the estimated porosity of 36%, 34%, 38% and 38% at initial, dry, brine saturated and fresh water saturated conditions, respectively. These estimations were based on the relationship that the bulk density equals the summation of the phase density multiplying the porosity and the saturation of that phase (including water phase and solid phase). The gas phase was neglected because its density is much less than the water and solid phases. These estimated porosities were all close to the porosity calculated gravimetrically of 36%. The differences between the estimated and actual initial water saturations and porosities can be caused by the assumptions used in the estimations, the resolution (0.195 mm x 0.195 mm x 0.625 mm voxel size) of the CT data used, and/or the imperfection of the bulk density or density change calibration from the raw CT data.

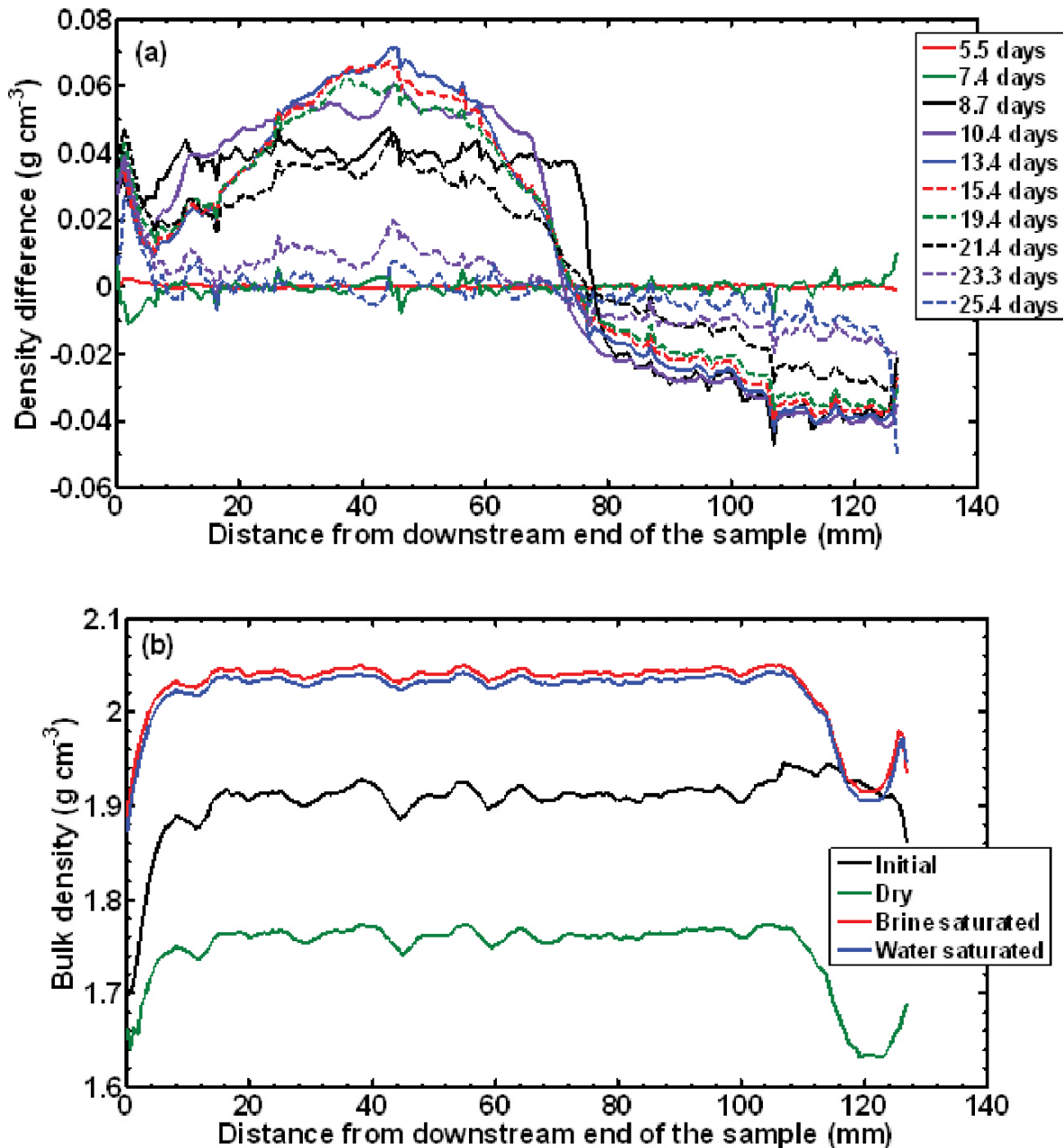


Figure 18: (a) Bulk density change from initial condition across the sample during methane hydrate formation and dissociation. (b) Bulk density across the sample at the initial pressure and temperature condition when the sample is filled with 49 vol.% brine and 51 vol.% methane gas, when the sample is saturated with brine, when the sample is saturated with fresh water and when the sample is dry and saturated with nitrogen. Bulk density and density change are the average values of all the pixels in one 0.625 mm slice that is scanned at each cross section perpendicular to the longitudinal axis of the sample.

Fig. 19 shows the calculated hydrate, water and gas phase saturation distributions across the sample during methane hydrate formation and dissociation. This calculation was based on Eqs. 8-10. On Days 5.5 and 7.4, the hydrate saturation was zero, and the water and gas saturations were relatively uniform across the sample. As hydrate formed, the hydrate saturation on the left side of the sample (greater than

40%) was greater than the right side (less than 40%) (Fig. 19(a)). The water saturation decreased across the sample; however, the decrease was greater in the right half (Fig. 19(b)). The gas saturation decreased to almost half of the initial value in the left half sample, while it slightly increased in the right side (Fig. 19(c)). Therefore, the bulk density in the left half of the sample increased (Figs. 19(a)) due to hydrate forming in some fraction of the pore space that was originally gas filled (Fig. 19). In contrast, the density on the right side decreased (Fig. 18(a)) due to an increase in gas saturation and reduction in brine saturation (Fig. 18). There must be some water migration from the right side to the left side. Otherwise, the formation of hydrate on the right side would increase the density there. As the sample temperature was increased, the phase saturations gradually returned to the initial distributions (Fig. 18).

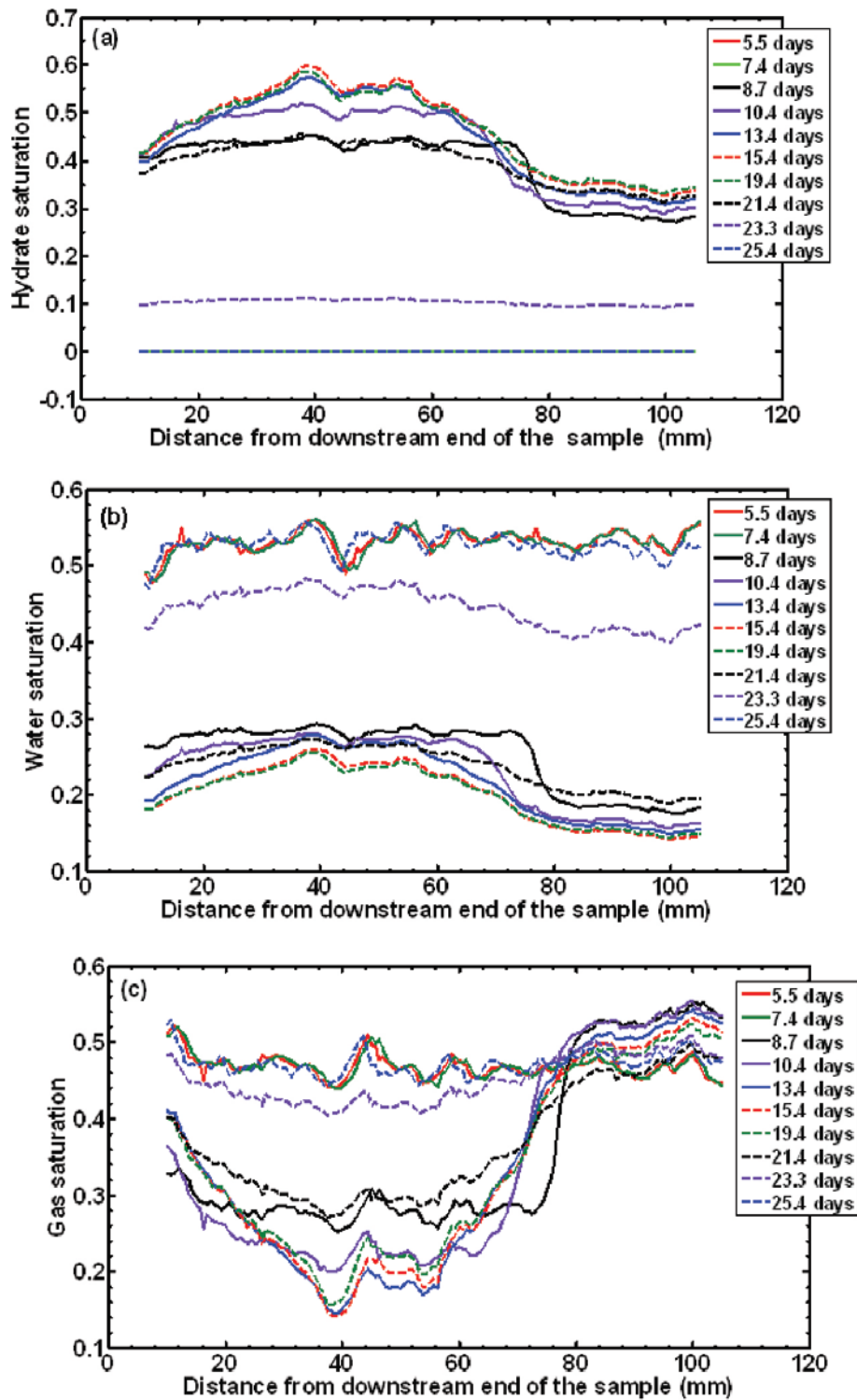


Figure 19: Calculated (a) hydrate, (b) water and (c) gas saturation distributions in the sample at different time of the experiment using the CT data in Fig. 18. The saturations between 0 and 10 mm, and between 105 and 127 mm are not presented because the sample was disturbed by inserting the endcap between 0-10 mm, and sand flowed out the sample between 105-127 mm.

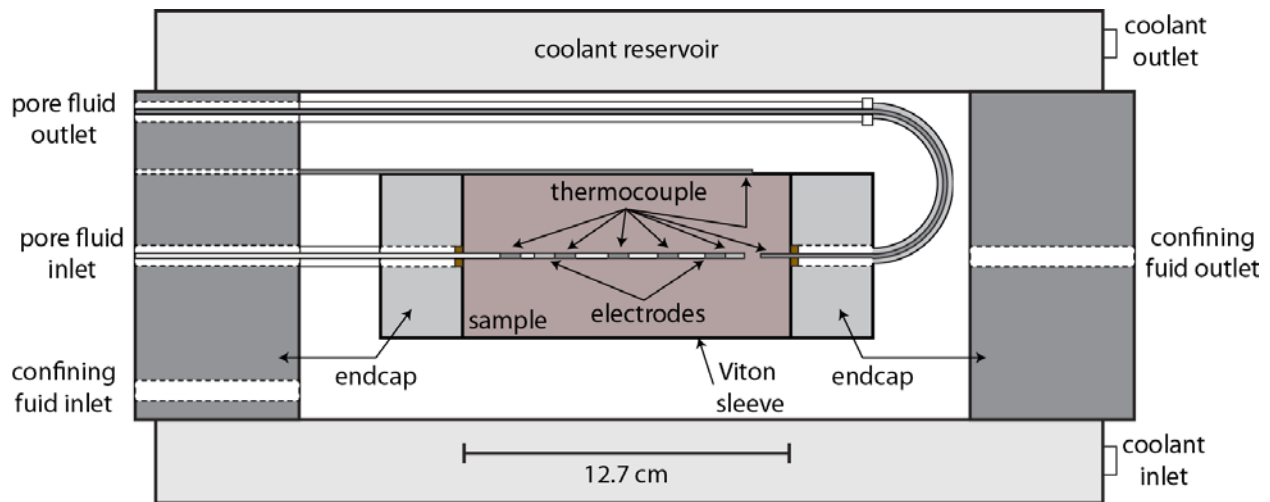
Status of winter 2014 experiment:

Figure 20: Experimental schematic for the second round of experiments. Note the additional four thermocouples mounted on the resistivity array.

We have now prepared the instrumentation for our next set of experiments, where we will test the modeling results outlined in the modeling section (1.22b). The new experimental set-up will be identical to the first one (Fig. 17), with the exception of the instrument string in the center of the sample. The new instrument string (Fig. 20) will consist of a resistivity array (two silver-silver chloride electrodes mounted on a garolite rod), but with four additional Type T thermocouples mounted to the garolite rod. With the addition of these thermocouples, we will measure temperature at approximately 1.25 cm, 3.8 cm, 6.4 cm, 8.9 cm, and 11.5 cm along the length of the core, in addition to the electrodes mounted at 2.5 cm and 10.0 cm. All other aspects of the experimental apparatus will be identical to the first experiment. As of 1 January 2014, the instrument string has been constructed, installed, and permanently mounted inside the pore fluid inlet tube. Remaining tasks include calibrating the electrodes and filling the sample holder with F-110 sand.

1.3 What opportunities for training and professional development has the project provided?

There has been strong interaction between UT and LBNL over this past quarter. Our graduate students and our post-doctoral scientist are now fully working with both institutions. A particularly ripe interface is that our students and post-doc are working closely with experimental efforts at LBNL. There is continuous interaction between petroleum engineering and geosciences as we address this problem.

1.4 How have the results been disseminated to communities of interest?

Darnell, K., Flemings, P.B., 2013, Methane hydrate destabilization sensitivity to physical complexity and initial conditions in a numerical model, Abstract OS21A-1622 presented at 2013 Fall Meeting, AGU, San Francisco, Calif., 9-13 Dec.

Darnell, K., Flemings, P.B., Bryant, S., 2014, Simulations of seafloor methane venting from warming-induced hydrate destabilization, Abstract submitted to be presented at *8th International Conference on Gas Hydrates* Beijing, China, 28 July to 1 August 2014.

DOE Award No.: DE-FE0010406

DUNS No.: 170230239

Quarterly Research Performance Progress Report (Period ending 12/31/2013)

CONTROLS ON METHANE EXPULSION DURING MELTING OF NATURAL GAS HYDRATE SYSTEMS: TOPIC AREA 2

Kneafsey, T., Flemings, P.B., Bryant, S., +You, K., +Polito, P., 2013, Preliminary Experimental Examination Of Controls On Methane Expulsion During Melting Of Natural Gas Hydrate Systems, Abstract C33A-0700 presented at 2013 Fall Meeting, AGU, San Francisco, Calif., 9-13 Dec

Meyer, D., Flemings, P.B., 2013, In situ gas hydrate saturation and salinity of hydrate-bearing sediments through well log analysis, Poster, Presented at the Society of Petrophysicists and Well Log Analysts Conference, New Orleans, LA, June 22-26.

Meyer, D., Flemings, P.B., 2013, Thermodynamic state of hydrate-bearing sediments on continental margins around the world, Abstract OS21A-1619 presented at 2013 Fall Meeting, AGU, San Francisco, Calif., 9-13 Dec

Meyer, D., Flemings, P.B., 2014, Thermodynamic State of Hydrate-Bearing Sediments on Continental Margins Around the World, Abstract submitted to be presented at *2014 Offshore Technology Conference*, Houston, TX, 5-8 May.

You, K., Flemings, P.B., Bryant, S., Kneafsey, T., Polito, P., 2014, Methane Hydrate Formation and Dissociation at Three-Phase Equilibrium at Constant Pressure, Abstract submitted to be presented at 8th International Conference on Gas Hydrates, Beijing, China, 28 July to 1 August 2014.

You, K., Flemings, P.B., Darnell, K., 2013, One Dimensional Advancing Solidification Front in the Hydrate System, Abstract OS13A-1686 presented at 2013 Fall Meeting, AGU, San Francisco, Calif., 9-13 Dec.

At the upcoming Gordon Research Conference on methane hydrates

(<http://www.grc.org/programs.aspx?year=2014&program=naturalgas>), the following will be attending:

1. Dylan Meyer
2. Kehua You
3. Kristopher Darnell

1.5 What do you plan to do during the next reporting period to accomplish the goals?

1.51 Task 1: Project Management and Planning:

Our core focus during the next quarter is to complete ongoing experimental work and to simulate melting of hydrate systems. We will continue with bi-monthly conference calls with Berkeley. We will continue to interact directly on experimental work. We will manage travel for visitations to Berkeley. We are completing reports for the contract.

1.52 Task 2: Conceptual and Numerical Model Development -1D:

Subtask 2.1 - Dissociation of 1D vertical hydrate accumulation

Subtask 2.2 - Apply 1D model to laboratory experiment

Subtask 2.3 - 1D models of natural examples

Subtask 2.3.1 Hydrate accumulations below permafrost

Subtask 2.3.2 - 1D model application to deposits near up-dip limit of stability zone on continental margins

Continue model development.

The only remaining task we have to do in 1D modeling is an analysis of hydrate melting below permafrost (Subtask 2.3.1) we are pursuing that now. All other subtasks were accomplished in the 12/2013 report.

1.53 Task 3: Categorize stability of known hydrate reservoirs:

We have complete and reported our analysis in the 12/2013 report. A paper on the approach was submitted to the OTC. We are currently writing up this work for publication.

1.54 Task 4: Laboratory Evaluation of Hydrate Dissociation:

Subtask 4.1 - Freezing to 3 phase stability conditions, followed by melting from above

Subtask 4.2 - Freezing to L+H condition, warming from above

Subtask 4.3 - Freezing to L+H condition, warming from below

We are currently pursuing these experiments at LBNL.

2 PRODUCTS:**2.1 What has the project produced?**

We have now produced a one dimensional, coupled; hydrate formation code that simulates the thermo-chemical response of a hydrate system to perturbation. We have demonstrated three phase stability through experimental analysis and we have modeled the behavior. We have also characterized the in-situ thermodynamic state of a number of hydrate locations around the world and shown that in at least two locations, local thermodynamic conditions are altered by high salinity.

3 PARTICIPANTS & OTHER COLLABORATING ORGANIZATIONS:**3.1 What individuals have worked on the project?**

Provide the following information for: (1) principal investigator(s)/project director(s) (PIs/PDs); and (2) each person who has worked at least one person month per year on the project during the reporting period, regardless of the source of compensation (a person month equals approximately 160 hours of effort).

Name	Peter Flemings	Steve Bryant	Tim Kneafsey	Dylan Meyer
Project Role	Principal Investigator	Co-Principal Investigator	Co-Principal Investigator	Graduate Student
Nearest person month worked	.25	.25	1.25	1
Contribution	Advised graduate student Meyer, managed project, and recruited students. Worked with technicians for thermistor development.	Advised graduate student Meyer on analysis of models of pore space alteration due to hydrate growth and its effect on saturation exponent.	Set up experiment, ran tests, and analyzed data.	Performed analysis of thermodynamic state of 3 locations.
Funding Support	The University of Texas	The University of Texas	Lawrence Berkeley National Lab	UTIG Fellowship
Collaborated	No	No	No	No

with individual in foreign country				
Name	Peter Polito	Kris Darnell	Kehua You	Tessa Green
Project Role	Laboratory Manager	Graduate Student	Post Doc	Project Coordinator
Nearest person month worked	1	1	1	1
Contribution	Participated in conference calls on experimental design. Ran experimental tests.	Performed literature review and theoretical calculation to prepare for laboratory experiments	Performed literature review and theoretical calculation to prepare for laboratory experiments	Coordinate meeting logistics, archive documents, and manage financials.
Funding Support	The University of Texas	The University of Texas	The University of Texas	The University of Texas
Collaborated with individual in foreign country	No	No	No	No

3.2 What other organizations have been involved as partners?

Organization Name: Lawrence Berkeley National Lab

Location of Organization: Berkeley, CA

Partner's contribution to the project (identify one or more)

- In-kind support: partner makes lab space and equipment available for experiments. (e.g., partner makes software, computers, equipment, etc., available to project staff);
- Facilities: Experiments are performed in partner's lab space using equipment largely supplied by the partner (e.g., project staff use the partner's facilities for project activities);
- Collaborative research: Partner collaborates with the project staff. (e.g., partner's staff work with project staff on the project); and

3.3 Have other collaborators or contacts been involved?

No

4 IMPACT:

4.1 What is the impact on the development of the principal discipline(s) of the project?

Geological models of gas transport and hydrate melting and solidification have suggested that free gas cannot migrate through the hydrate stability zone during melting. In contrast, we suggest that free gas can migrate through the hydrate stability zone by altering the conditions of hydrate stability to a state of three-phase equilibrium through the elevation of salinity and possibly temperature. This results in

fundamentally different macro-scale behavior during melting and may result in greater gas venting than has been previously demonstrated. If this hypothesis is correct, it may engender a new generation of field and laboratory investigations to document this behavior in both the field of geosciences and petroleum engineering. Second, the project links theoretical development with laboratory modeling because the concepts can be applied at the laboratory scale as well as the field scale. The laboratory experiments to be conducted will enable validation of the mechanisms incorporated in the models. These laboratory experiments will play a key role in demonstrating the processes.

4.2 What is the impact on other disciplines?

A likely outcome of our work is a more quantitative prediction of the magnitude of methane flux from the earth to the atmosphere over human (decadal) timescales and geological timescales (10,000 years). These will serve as boundary conditions for atmospheric climate models. In turn, these results may guide policy decisions.

4.3 What is the impact on the development of human resources?

We are working at the interface of geosciences and engineering. We are coupling theory and laboratory experiments to address macro-scale geologic problems. This is training a new generation of geoscientists and engineers to think with a systems-based approach that links observation with theory.

The results are being applied in the classroom and the support is training several graduate students.

4.4 What is the impact on physical, institutional, and information resources that form infrastructure?

The project is strengthening the experimental efforts and capability at UT as it is our job to develop sensor equipment. The project is strengthening development at LBNL where primary experimental work is occurring.

4.5 What is the impact on technology transfer?

We are presenting our research to approximately 100 industry members at our GeoFluids consortium and we will be presenting at a range of national and international meetings. We will also present our results at the upcoming OTC conference in Spring 2014.

4.6 What is the impact on society beyond science and technology?

A likely outcome of our work is a more quantitative prediction of the magnitude of methane flux from the earth to the atmosphere over human (decadal) timescales and geological timescales (10,000 years). These will serve as boundary conditions for atmospheric climate models. In turn, these results may guide policy decisions.

4.7 What dollar amount of the award's budget is being spent in foreign country(ies)?

Zero percent of the award's budget is being spent in foreign countries.

5 CHANGES/PROBLEMS:

5.1 Changes in approach and reasons for change

We have made some changes in our specific experimental approaches. The original experimental tasks were described as follows:

Task 4: Laboratory Evaluation of Hydrate Dissociation:

Subtask 4.1 - Freezing to 3 phase stability conditions, followed by melting from above

Subtask 4.2 - Freezing to L+H condition, warming from above

Subtask 4.3 - Freezing to L+H condition, warming from below

However, after experimental planning and theoretical modeling over the last quarter, we decided that the most important first step in the modeling would be to 1) demonstrate the ability to create three phase conditions in the laboratory and 2) show the effects of perturbation on this material. After establishing this capability, we would then demonstrate the effects of thermal perturbation from above or below and have developed the ability to do so even in the smaller sample.

We will still be able to meet our Milestone **1.E**, 'Demonstrate ability to create and dissociate methane hydrate within sediment columns under conditions analogous to natural systems.'

There are no other changes in approach to report for this reporting period.

5.2 Actual or anticipated problems or delays and actions or plans to resolve them

No problems or delays to report for this reporting period.

5.3 Changes that have a significant impact on expenditures

No changes in approach to report for this reporting period.

5.4 Significant changes in use or care of human subjects, vertebrate animals, and/or Biohazards

Nothing to report

5.5 Change of primary performance site location from that originally proposed

Nothing to report

6 BUDGETARY INFORMATION:

Approved budget from original proposal for budget period 2 is outlined in table 1.

Object Class Categories	Grant Program, Function or Activity Total (5)		
	(1) DOE Funds	(2) Cost Share	
a. Personnel	\$ 204,175.00	\$ 60,475.00	\$ 264,650.00
b. Fringe Benefits	\$ 55,127.00	\$ 16,328.00	\$ 71,455.00
c. Travel	\$ 6,252.00		\$ 6,252.00
d. Equipment			\$ -
e. Supplies	\$ 5,400.00		\$ 5,400.00
f. Contractual	\$ 64,039.00		\$ 64,039.00
g. Construction			\$ -
h. Other	\$ 24,717.00	\$ 17,917.00	\$ 42,634.00
i. Total Direct Charges (sum of 6a-6h)	\$ 359,710.00	\$ 94,720.00	\$ 454,430.00
j. Indirect Charges	\$ 149,986.00	\$ 41,474.00	\$ 191,460.00
k. Totals (sum of 6i-6j)	\$ 509,696.00	\$ 136,194.00	\$ 645,890.00

Table 1: Approved budget for Budget Period 2

Our project is on track to complete the objectives as originally proposed and expend the total estimate included in the original proposal. Budget Period 2 spending is outlined in Table 1. The vast majority of the 18% that will not be spent in Budget Period 1 is \$53,988 in salary (federal share = \$39045, non-federal share=\$14,943) (Table 2)). We will use these monies to further our experimental work by supporting UT Research Associate Peter Polito. Polito has been spending extensive periods of time assisting experimentation at LBNL. Our experimental work has proceeded more slowly than we had hoped and this will help us achieve our Budget Period 2 goals.

	Budget Period 2	Budget Period 1	Projected Spending	Remaining
<i>Federal Share</i>				
SALARIES & WAGES	\$ 204,175.00	\$ 39,045.00	\$ (243,220.00)	\$ -
FRINGE BENEFITS	\$ 55,127.00	\$ 13,847.14	\$ (68,974.14)	\$ -
MATERIAL AND SUPPLIES	\$ 5,400.00	\$ -	\$ (5,400.00)	\$ -
LAPTOP	\$ -	\$ -	\$ -	\$ -
PUBLICATIONS	\$ 5,000.00	\$ 5,000.00	\$ (10,000.00)	\$ -
LAWRENCE BERKELEY NAT'L LAB	\$ 64,039.00	\$ -	\$ (64,039.00)	\$ -
COMPUTER COST	\$ 1,800.00	\$ -	\$ (1,800.00)	\$ -
TUITION	\$ 17,917.00	\$ 8,635.00	\$ (26,552.00)	\$ -
TRAVEL-DOM	\$ 6,252.00	\$ -	\$ (6,252.00)	\$ -
OVERHEAD	\$ 149,986.00	\$ 42,499.87	\$ (192,485.87)	\$ -
Total	\$ 509,696.00	\$ 109,027.15	\$ (618,723.01)	\$ -
<i>Non-Federal Share</i>				
SALARIES & WAGES	\$ 60,475.00	\$ 14,943.25	\$ (75,418.25)	\$ -
FRINGE BENEFITS	\$ 16,328.00	\$ 4,034.79	\$ (20,362.79)	\$ -
TUITION	\$ 17,917.00	\$ 9,133.67	\$ (27,050.67)	\$ -
OVERHEAD	\$ 41,474.00	\$ 10,248.96	\$ (51,722.96)	\$ -
Total	\$ 136,194.00	\$ 38,360.67	\$ (174,554.67)	\$ -
Project Total	\$ 645,890.00	\$ 147,387.82	\$ (793,277.68)	\$ -

Table 2: Projected spending budget period 2. Budget Period 1 funds show the amount of money carried over from Budget Period 1. These monies will be applied during Budget Period 2 to support our experimental work in cooperation with LBNL.

7 References

- Archie, G. E. (1941) The electrical resistivity log as an aid in determining some reservoir characteristics. *Transactions of AIME*, 146, 9.
- Arps, J. J. (1953) The Effect of Temperature on the Density and Electrical Resistivity of Sodium Chloride Solutions. *Society of Petroleum Engineers*, 5, 4.
- Bily, C. & J. W. L. Dick (1974) Naturally occurring gas hydrates in the Mackenzie Delta, N.W.T. *Bulletin of Canadian Petroleum Geology*, 22, 340-352.
- Collett, T. S. & S. R. Dallimore. 1998. Quantitative assessment of gas hydrates in the Mallik L-38 well, Mackenzie Delta, NWT, Canada. In *Proceedings of the Eighth International Conference on Permafrost, June 23-27, 1998*, eds. A. G. Lewkowicz & M. Allard, 6. Quebec, Quebec: Centre d'etudes nordiques.

- Collett, T. S., R. E. Lewis & S. R. Dallimore. 2005. JAPEX/JNOC/GSC et al. Mallik 5L-38 gas hydrate production research well downhole well-log and core montages. In *Scientific Results from the Mallik 2002 Gas Hydrate Production Research Well Program, Mackenzie Delta, Northwest Territories, Canada*, ed. S. R. Dallimore, and Collett, T. S., 23. Geological Survey of Canada.
- Cook, A. E., B. I. Anderson, J. Rasmus, K. Sun, Q. Li, T. S. Collett & D. S. Goldberg (2012) Electrical anisotropy of gas hydrate-bearing sand reservoirs in the Gulf of Mexico. *Marine and Petroleum Geology*, 34, 72-84.
- Dallimore, S. R., T. Uchida & T. Collett. 1999. Summary. In *Scientific results from JAPEX/JNOC/GSC Mallik 2L-38 Gas Hydrate Production Research Well, Mackenzie Delta, Northwest Territories, Canada, Volume Bulletin 544, Geological Survey of Canada*, eds. S. R. Dallimore, T. Uchida & T. S. Collett, 10.
- Duan, Z., N. Møller, J. Greenberg & J. H. Weare (1992) The prediction of methane solubility in natural waters to high ionic strength from 0 to 250°C and from 0 to 1600 bar. *Geochimica et Cosmochimica Acta*, 56, 1451-1460.
- Expedition 311 Scientists. 2006. Site U1328. In *Proceedings of the Integrated Ocean Drilling Program*, eds. M. Riedel, T. S. Collett, M. J. Malone & Expedition 311 Scientists. Washington, DC (Integrated Ocean Drilling Program Management International, Inc.).
- Henry, P., M. Thomas & M. Ben Clennell (1999) Formation of natural gas hydrates in marine sediments 2. Thermodynamic calculations of stability conditions in porous sediments. *Journal of Geophysical Research*, 104, 23005-23022.
- IOC, IHO & BODC. 2003. Centenary Edition of the GEBCO Digital Atlas, published on CD-ROM on behalf of the Intergovernmental Oceanographic Commission and the International Hydrographic Organization as part of the General Bathymetric Chart of the Oceans, British Oceanographic Data Centre, Liverpool, U.K.
- Liu, X. & P. B. Flemings (2006) Passing gas through the hydrate stability zone at southern Hydrate Ridge, offshore Oregon. *Earth and Planetary Science Letters*, 241, 211-226.
- Lu, H., R. Dutrisac, J. Ripmeester, F. Wright & T. Uchida. 2005. Measurements of gas hydrate saturation in sediment cores recovered from the JAPEX/JNOC/GSC et al. Mallik 5L-38 gas hydrate production research well. In *Scientific Results from the Mallik 2002 Gas Hydrate Production Research Well Program, Mackenzie Delta, Northwest Territories, Canada*, eds. S. R. Dallimore & T. S. Collett, 11.
- Malinverno, A., M. Kastner, M. E. Torres & U. G. Wortmann (2008) Gas hydrate occurrence from pore water chlorinity and downhole logs in a transect across the northern Cascadia margin (Integrated Ocean Drilling Program Expedition 311). *Journal of Geophysical Research: Solid Earth*, 113, B08103.
- Matsumoto, R., H. Tomaru, Y. F. Chen, H. Lu & I. D. Clark. 2005. Geochemistry of the interstitial waters of the JPAX/JNOC/GSC et al. Mallik 5L-38 gas hydrate production research well. In *Scientific Results from the Mallik 2002 Gas Hydrate Production Research Well Program, Mackenzie Delta, Northwest Territories, Canada*, eds. S. R. Dallimore & T. S. Collett, 11.
- Medioli, B. E., N. Wilson, S. R. Dallimore, D. Pare, P. Brennan-Alpert & H. Oda. 2005. Sedimentology of the cored interval, JAPEX/JNOC/GSC et al. gas hydrate production research well. In *Scientific Results from the Mallik 2002 Gas Hydrate Production Research Well Program, Mackenzie Delta, Northwest Territories, Canada*, eds. S. R. Dallimore & T. S. Collett, 14.
- Milkov, A. V., Y.-J. Lee, W. S. Borowski, M. E. Torres, W. Xu, H. Tomaru, A. M. Trehu, P. Schultheiss, G. R. Dickens & G. E. Claypool (2004) Co-existence of gas hydrate, free gas, and brine within the regional gas hydrate stability zone at Hydrate Ridge (Oregon margin): Evidence from prolonged degassing of a pressurized core. *Earth and Planetary Science Letters*, 222, 829-843.

- NGHP Expedition 01 Scientists. 2007. Sites NGHP-01-10, 12, and 13. In *National Gas Hydrate Program Expedition 01 Initial Reports, Directorate General of Hydrocarbon, Ministry of Petroleum and Natural Gas (India)*, eds. T. S. Collett, M. Reidel, J. Cochran, R. Boswell, J. Presley, P. Kumar, A. Sathe, A. Sethi, M. Lall & the NGHP Expedition 01 Scientists, 150.
- Seol, Y. & T. J. Kneafsey (2011) Methane hydrate induced permeability modification for multiphase flow in unsaturated porous media. *Journal of Geophysical Research: Solid Earth*, 116, B08102.
- Shipboard Scientific Party. 2003. Site 1249. In *Proceedings of the Ocean Drilling Program, Initial Reports*, eds. A. M. Trehu, G. Bohrmann, F. R. Rack, M. E. Torres & et al. College Station: Ocean Drilling Program.
- Spangenberg, E. (2001) Modeling of the influence of gas hydrate content on the electrical properties of porous sediments. *Journal of Geophysical Research: Solid Earth*, 106, 6535-6548.
- Takahashi, H., E. Fercho & S. R. Dallimore. 2005. Drilling and operations overview of the Mallik 2002 Production Research Well Program. In *Scientific Results from the Mallik 2002 Gas Hydrate Production Research Well Program, Mackenzie Delta, Northwest Territories, Canada*, ed. S. R. Dallimore, and Collett, T. S., 14. Geological Survey of Canada.

Nomenclatures

Cl_e	salinity at three phase equilibrium (wt.%)
Cl_i	initial salinity (wt.%)
C_{i-s}	in-situ salinity (wt.%)
CT_{dry}	bulk density from CT scans at the dry condition ($kg\ m^{-3}$)
CT_e	bulk density at the condition to be estimated ($kg\ m^{-3}$)
CT_{sat}	bulk density from CT scans at brine saturated condition ($kg\ m^{-3}$)
D^m	salt effective diffusion coefficient in water phase in the sample ($m^2\ sec^{-1}$)
f	mass ratio of the hydrate to water in methane hydrate ($f=1.15$)
L	length of the sample (m)
L_{dif}	distance from the hydrate solidification front where salinity equals the initial value (m)
M_h	methane hydrate molecular weight ($0.106\ kg\ mol^{-1}$)
M_m	methane molecular weight ($0.016\ kg\ mol^{-1}$)
q_m	methane injection rate ($kg\ m^{-2}\ sec^{-1}$)
S_h	hydrate saturation (dimensionless)
S_T	total saturation of water and hydrate on the water basis (dimensionless)
S_w	water saturation (dimensionless)
T_e	three phase equilibrium temperature at initial pressure and salinity condition (oC)
T_{exp}	experimental temperature ($^{\circ}C$)
t_e	time for the whole sample to reach three phase equilibrium (sec)
X	fraction of initial water converted into hydrate (dimensionless)
ϕ	porosity of the sample
ρ_h	methane hydrate density ($912\ kg\ m^{-3}$)
ρ_w	water phase density ($kg\ m^{-3}$)
a	tortuosity coefficient (dimensionless)
m	cementation exponent (dimensionless)
N	saturation exponent (dimensionless)
F	formation factor (dimensionless)
R_w	pore water resistivity (ohmm)
R_t	formation resistivity (ohmm)

National Energy Technology Laboratory

626 Cochrans Mill Road
P.O. Box 10940
Pittsburgh, PA 15236-0940

3610 Collins Ferry Road
P.O. Box 880
Morgantown, WV 26507-0880

13131 Dairy Ashford Road, Suite 225
Sugar Land, TX 77478

1450 Queen Avenue SW
Albany, OR 97321-2198

Arctic Energy Office
420 L Street, Suite 305
Anchorage, AK 99501

Visit the NETL website at:
www.netl.doe.gov

Customer Service Line:
1-800-553-7681

